N. Jb. Geol. Paläont. Abh. 273/1 (2014), 89–120
Stuttgart, July 2014

Article

Origin and evolution of metamorphosed mantle peridotites of Darreh Deh (Nain Ophiolite, Central Iran): Implications for the Eastern Neo-Tethys evolution

Nargess Shirdashtzadeh, Ghodrat Torabi, Thomas Meisel, Shoji Arai, Syed Nadeem Hussain Bokhari, Ramin Samadi, and Esteban Gazel

With 11 figures and 8 tables

Abstract: The Nain Ophiolite is one of the most complete harzburgitic-ophiolite suites exposed along the Nain-Baft Fault, around the Central-East Iranian Microcontinent (CEIM). It is a remnant of the Nain Ocean (Early Jurassic to upper Early Cretaceous-Paleocene). During the Cretaceous (~Albian to Cenomanian), ascending melts and serpentinization overprinted the Jurassic melt-rock reactions and metamorphism of peridotites in most of the ophiolite. However, metamorphosed peridotites of the Darreh Deh massif in the eastern part of Nain Ophiolite remained intact, with the lowest degree of alteration and serpentinization and slightly higher degrees of partial melting and melt – rock reactions. Clinopyroxene and Cr-spinel compositions together with bulk rock geochemistry of Darreh Deh peridotites indicate a mid-ocean ridge affinity for lherzolite but later compressional tectonics led to an intra-oceanic subduction and supra-subduction zone (SSZ) in which harzburgite and dunite formed due to ascending melt reacting with the mantle lherzolite. Further indications are the presence of replacive olivine, incongruent melting of orthopyroxene and increase of Cr# of Cr-spinel in harzburgite. The extensional to compressional evolution in the Jurassic ended with accretionary and/or collisional processes induced by convergence between the Sanandaj – Sirjan zone and the CEIM. These caused a regional metamorphism that affected the Darreh Deh massif by forming antigorite, talc, metamorphic olivine, tremolite and chlorite metamorphic assemblages in mantle peridotites at amphibolite facies (~630-700 °C / 7-15 kbar) conditions, similar to the metamorphosed diabasic dikes, basalts and pillow lavas of this ophiolite.

Key words: ophiolite, Central Iran, Nain, melt-rock reaction, metamorphosed mantle peridotite.

---

1. Introduction

Petrography coupled with in situ mineral chemistry allows us to investigate the nature and condition of melt-rock reactions and to constrain some aspects of the melting history of peridotites (Seyler et al. 2007). However, the emplacement of peridotite into, or onto, continental crust can result in changes in its mineralogical, structural, textural and bulk chemical properties (Evans 1977) both prior to and during emplacement, and subsequent crustal deformation and metamorphism (Bucher & Grapes 2011). Metamorphism of peridotite and serpentinite has been examined in detail by previous workers (e.g. Evans 1977, Bucher & Grapes 2011; Coleman 1977; Nicolas 1989; Dilek & Newcomb 2003; Torabi et al. 2011a). Many of the original properties of peridotite are affected by the metamorphism, but the geochemistry of selected primary igneous minerals (e.g. relics of clinopyroxene and Cr-spinel) may be used to reconstruct the original character of the metamorphosed peridotite protolith.

Evidence from abyssal peridotites suggests that mechanisms other than the expected fractional crystallization, such as significant reaction of melt with shallow mantle peridotite beneath mid-ocean ridges, can occur during the early stages of cooling and crys-

DOI: 10.1127/0077-7749/2014/0418
www.schweizerbart.de
0077-7749/2014/0418 $ 8.00

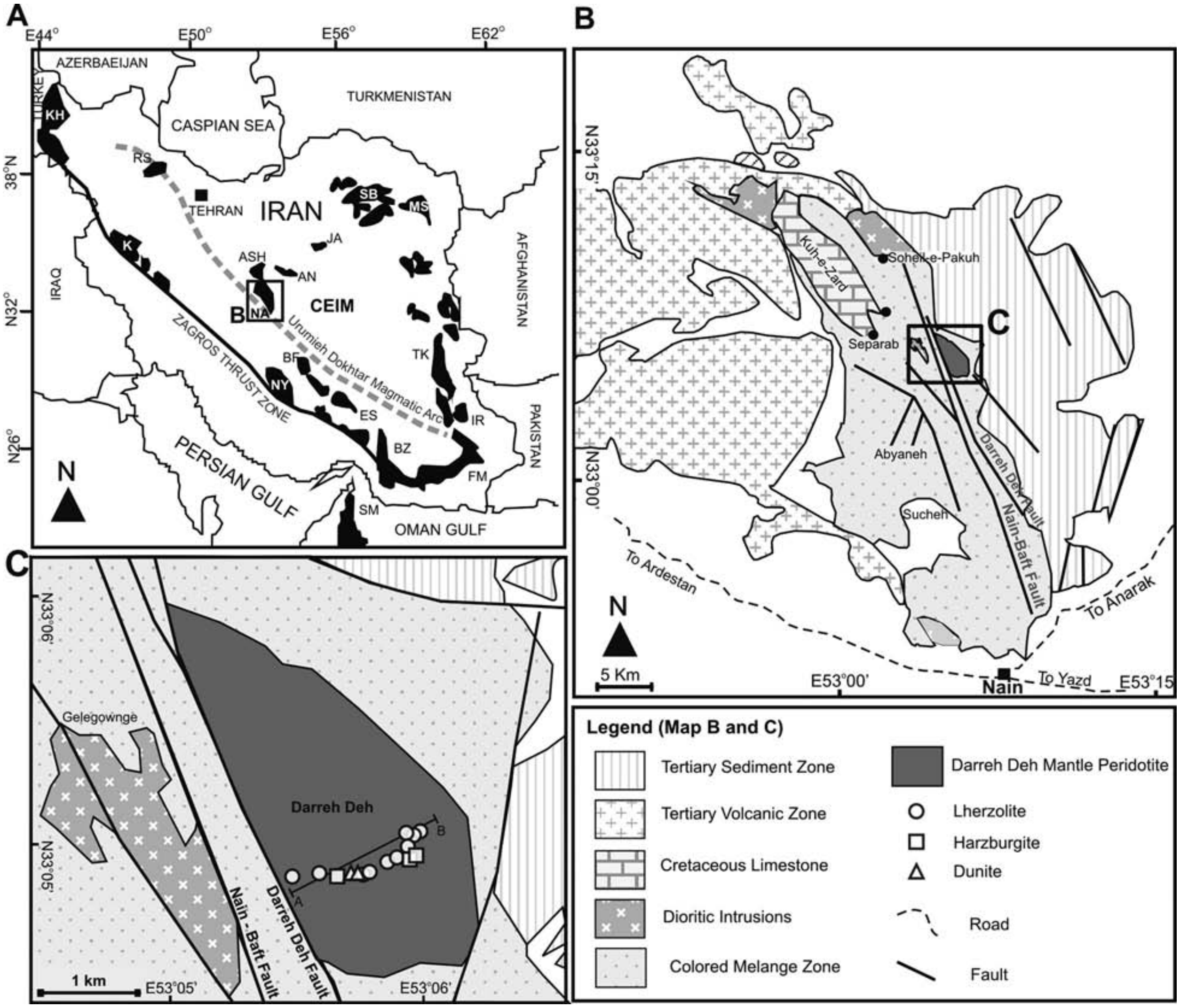

Fig. 1. (A) Distribution of the main ophiolites in Iran including the study area situated within the Nain Ophiolite (ophiolite abbreviations: NA=Nain, ASH-ZA = Ashin-Zavar, AN = Anark, MS = Mashhad, SB = Sabzevar, KH = Khoy, TK = Tchehel Kureh, NY = Neyriz, IR = Iranshahr, K = Kermanshah, BZ = Band-e-Ziarat, ES = Esfandagheh, BF = Baft, SM = Semail, FM = Fanuj-Maskutan, JA = Jandagh); (B) Simplified geological map of the Nain Ophiolitic mélange to the north of Nain city (modified from Davoudzadeh 1972); (C) The Darreh Deh massif with sample locations of the metamorphosed peridotites.

tallization of mid-ocean ridge basalt (MORB) magmas. This process is known as “reactive crystallization”, meaning crystallization influenced by melt-rock reaction (Collier & Keleman 2010). Harzburgite may result from interaction between a protolith and melts (i.e., “reactive” harzburgite). During this reaction, percolating melt preferentially dissolved clinopyroxene and orthopyroxene and precipitated olivine, transforming the lherzolite (clinopyroxene-bearing) into harzburgite (clinopyroxene-poor) (Xu et al. 2003).

Jurassic oceanic crust around the CEIM (Central-East Iranian Microcontinent) and in the Inner Zagros Ophiolitic Belt is rare or unknown, herein we focus on rare oceanic crust occurring around the CEIM to trace melt-rock reactions and metamorphism in mantle peridotites that occurred before Cretaceous.

Several recent papers deal with the peridotites (harzburgite, lherzolite, dunite) and chromitite in the Nain Ophiolite (e.g. Pirnia et al. 2010; Torabi 2008; Ghazi et al. 2011), but no scientific work was done on the metamorphosed mantle peridotites. Cretaceous melt-rock reactions in the mantle peridotites in the central parts of the Nain Ophiolite are also considered in many papers, but here we studied in detail the mantle peridotites of Darreh Deh in order to trace melt-rock reactions that took place before the Cretaceous.

This work is the first study on Darreh Deh metamorphosed mantle peridotites of the Nain Ophiolite and it addresses the effects of regional amphibolite-facies metamorphism on the mantle peridotites of the Nain Ophiolite, using petrology and geochemistry, in addition to the pre-Cretaceous melt-rock reactions relics in the mantle peridotites of this ophiolite. This study is a consequential study that provides important constraints on the evolution of the Nain Ophiolite and the CEIM, and its results can be transferred to many other worldwide ophiolites with comparable evolutions of mantle melting processes, multi-stage magmatism and metamorphism.

2. Geological background

In the Early Permian to Middle Permian - Early Triassic, the western Cimmerian terranes of present-day Iran migrated from southern Gondwana as a consequence of the opening of the western branch of Neo-Tethys Ocean between the Iranian and Arabian plates (e.g. AGARD et al. 2011, and references therein). The closure of this Triassic ocean in Upper Cretaceous times resulted in the formation of the Kermanshah to Neyriz and Oman ophiolites, and the Eocene - Miocene Urumieh Dokhtar magmatic arc (UDM) to the west of the Nain and Ashin ophiolitic mélanges (Fig. 1A). Much petrological evidence indicates that the eastern branch of the Neo-Tethys ocean (MUTTONI et al. 2009) or Nain-Baft Ocean (in GHASEMI & TALBOT 2006; SHIRDASHTZADEH et al. 2011) was a long–lived ocean (~Early Jurassic to Upper Cretaceous) and predates Upper Cretaceous subduction in the western branch of the Neo-Tethys and predated Neo-Tethys subduction beneath the Sanandaj-Sirjan zone. The evidence is (1) Early Jurassic to Upper Cretaceous plagiogranite relics from this oceanic suite (SHARKOVSKI et al. 1984), (2) early Upper Cretaceous radiolarian cherts (SHIRDASHTZADEH 2014) and limestones (SHARKOVSKI et al. 1984), (3) early Upper Cretaceous hornblende gabbro (HASSANIPAK & GHAZI, 2000), which are all older than the Eocene – Miocene UDM in the west of the Nain Ophiolite. Therefore, GLENNIE (1992), TORABI (2004), REICHERT (2007), SHIRDASHTZADEH et al. (2010, 2011) considered the Nain Ocean as the eastern branch of the Neo-Tethys Ocean, which opened from southeast Turkey to Oman and separated the Sanandaj-Sirjan and Central Iranian plates from the Early Jurassic to the upper Early Cretaceous-Paleocene (~150 to 100 Ma). Basin closure resulted in the formation of the Ashin and Nain Ophiolites.

The age of the opening of the eastern branch of the Neo-Tethys Ocean is not well constrained. However, SHARKOVSKI et al. (1984) obtained 188 Ma (Pliensbachian in Early Jurassic) and 98 Ma (Cenomanian in Early Upper Cretaceous) K-Ar ages for two melting stages (gabbro-plagiogranite in Table 1) from the Ashin (= Ashin-Zavar) ophiolite, which shares the same suture zone and has a history comparable to the Nain Ophiolite (SHIRDASHTZADEH et al. 2011). In addition, judging from the presence of metamorphosed and not-metamorphosed basic rocks, SHIRDASHTZADEH (2007, 2014) and SHIRDASHTZADEH et al. (2010, 2011) proposed that extensional processes leading to the formation of Nain – Baft oceanic crust occurred during at least two phases. The first phase occurred in the Early Jurassic, when Nain oceanic crust segments started to form due to spreading. Melting of an ancient primary mantle lherzolite produced diabasic dikes and pillow lavas which were subsequently covered by pelagic sediments. Prograde regional metamorphism during closure and tectonism of this oceanic realm around the middle Jurassic turned these rocks into orthoamphibolites (at ~650-800 °C / 7-8 kbar; SHIRDASHTZADEH et al. 2010), metachert, skarn and schist. However, uncertainties still exist as to whether this high-grade Jurassic metamorphism left any imprints on the mantle peridotite of this ophiolite, because they have undergone widespread severe alteration and serpentinization or were affected by melt–rock reactions.

Oceanic spreading resumed in the Cretaceous producing sheeted dikes, massive basalts, and basaltic pillow lavas with a MORB signature (SHIRDASHTZADEH et al. 2011). These were covered by radiolarian cherts and Globotruncana limestones of late Cretaceous age (TORABI et al. 2011b) and, in the east, by the Middle Eocene–Lower Oligocene Akhoreh Formation (SHARKOVSKI et al. 1984).

The 188 Ma age of the plagiogranites (SHARKOVSKI et al. 1984, Table 1) is in agreement with Jurassic magmatism and the younger 98 Ma age (SHARKOVSKI et al. 1984, Table 1) for a later phase of magmatism in the Cenomanian (at the beginning of the Upper Cretaceous), when the Nain oceanic spreading system reactivated melt-rock reaction and production of basalts, diabasic dikes and gabbros. The latter magmatic phase is also supported by three $^{40}Ar/^{39}Ar$ ages of 101.2 ± 0.9, 99.7 ± 0.9, 99 ± 1.2 Ma (~Albian, in upper term of Lower Cretaceous) obtained for hornblende gabbros from the Nain Ophiolite (Hassanipak & Ghazi 2000) and K-Ar dating of amphibole in gabbro (by Moghadam et al. 2009) that yields an age of 93.4 ± 3.6 Ma (Cenomanian) (Table 1). In addition, U-Pb zircon ages of Nain plagiogranite (102-103 Ma) are comparable to the 98 Ma K-Ar age for gabbro-plagiogranite (Table 1) of the Ashin ophiolite to the northeast (Moghadam et al. 2013).

The uppermost magmatic units of the Nain Ophiolite (basalts and pillow lavas) are covered by upper Early Cretaceous to Paleocene and Early Eocene sediments, themselves part of the mélange. These sediments are intruded by Eocene intrusive rocks that are not part of the mélange. As the Akhoreh Formation (flysch) was deposited during and after Eocene volcanism (Torabi 2010), the closing of the Nain Ocean definitely occurred during, or sometime after the upper Early Cretaceous to Paleocene, and before the Eocene, as reported for other Neo-Tethyan Ocean relics around the CEIM (e.g. the Sistan micro-ocean to the east of the CEIM, Bröcker et al. 2013).

2.1. Nain Ophiolite

The Mesozoic ophiolitic mélange of Nain (or Naein) occurs to the north of Nain city (Isfahan Province) and is exposed in a 15 km wide and 35 km long area situated at the western end of the CEIM, along the Sabzevar to Nain-Baft faults (Fig. 1A). The Nain ophiolitic mélange consists of a chaotic mixture of igneous, metamorphic and sedimentary rocks. It is mainly composed of harzburgite, lherzolite and dunite and their serpentinized varieties. Other rock units are chromitite, pyroxenite, gabbro, diabasic dike, spilitized pillow lava, and plagiogranite, in addition to a wide variety of metamorphic rocks, including metamorphosed mafic rocks (amphibolite), schist, skarn, marble, rodingite, metachert and listwaenite; all form part of a metamorphosed oceanic crust unit (Shirdashtzadeh 2007, 2014, Shirdashtzadeh et al. 2010, 2011).

During their complex tectonic history of obduction and emplacement these rock units were mixed to form an ophiolite mélange. However, amphibolitic rocks of the Nain ophiolite are mostly exposed along the suture zone, in Soheil-e-Pakuh, Abyaneh-e-Nain, south of Separab, south of Kuh-e-Zard, and near the Soucheh farm (Fig. 1B). Some amphibolites formed from basalts and basic pillow lavas of the Nain ophiolite sequence and have a massive appearance, while some are regionally metamorphosed primary diabasic dykes within the mantle peridotites (Shirdashtzadeh et al. 2010). However, relics of amphibolite facies metamorphism in the mantle peridotite host were overprinted and removed during later alteration during mélange formation. Most harzburgites and dunites in the central parts of the Nain Ophiolite are the products of Cretaceous rock-melt reactions triggered by ascending melts, causing incongruent melting of orthopyroxene in ~Albian to Cenomanian times, as is clear from the formation of secondary olivine with lower Mg# and increasing Cr# of Cr-spinel, compared to those in associated mantle lherzolite (Pirnia 2007).

2.2. Study area: Darreh Deh massif

The study area of Darreh Deh massif is exposed in the eastern part of the Nain Ophiolite (N33º04' to 06' and E53º05' to 06.3') along the active right-lateral strike slip Darreh Deh Fault (Nadimi & Sohrabi 2008) and along the Nain-Baft Fault in the west (Fig. 1C). The massif is dominated by metamorphosed mantle lherzolite, clinopyroxene-bearing harzburgite, and harzburgite, but small volumes of dunite, metapicrite and metarodingite are also present. This massif that is an isolated exposure, contrasting with other mantle peridotites in the central part of the Nain Ophiolite by its darker color, higher topographic relief, smaller number of basic intrusives, lower serpentinization degree, and amphibolite-facies metamorphism. This study is the first detailed study of this region, and focusses on the petrology of the metamorphosed peridotites.

3. Analytical methods

Quantitative chemical analyses of mineral compositions (Tables 2 to 6) were carried out using a JEOL JXA8800R wavelength-dispersive electron probe micro-analyzer at the Centre for Cooperative Research of Kanazawa University (Kanazawa, Japan). The analyses were performed with an accelerating voltage of 15 kV and a beam current of 15 nA. Standard corrections of atomic (Z) number factors (= ZAF) were carried out. Natural and synthetic minerals of known composition were used for calibration. Abbreviations of mineral names are adopted from Whitney & Evans (2010). The Fe^{3+} content of minerals was estimated by assuming mineral stoichiometry (Droop 1987).

The major, trace and rare earth element contents of clinopyroxene from Darreh Deh lherzolite were obtained by laser ablation ICP-MS (LA-ICP-MS) using an ArF 193 nm Excimer Laser coupled to an Agilent 7500S at the Earth Science Department of the Kanazawa University (Japan). The diameter of the analyzed points was 60 micrometers at a frequency of 5 Hz. The standard synthetic glass NIST SRM 612 (PEARCE et al. 1997) was used for calibration with ^{29}Si as an internal standard. The concentrations of La, Ce, Pr, Ta, Pb and Th were below the detection limits (Table 6).

For the determination of major and trace element contents, a combination of X-ray fluorescence (XRF) analysis, and sodium peroxide sintering with ICP-MS analysis was selected. The method largely follows that of MEISEL et al. (2002), in particular to assure complete digestion of chromite bearing peridotites. In brief, 100 mg sample powder was mixed with 600 mg finely ground Na_2O_2, sintered, and dissolved in 3 mol/l HCl. The final dilutions for the ICP-MS measurements were 1:5000; measurements were carried out using an Agilent 7500cx at the Montanuniversität, Leoben, Austria. Quantifications of the signal were done with external calibrations on certified and non-certified geological reference materials (Table 7).

Serpentine minerals were identified by micro-Raman spectroscopy at Kanazawa University using a HORIBA Jobin Yvon, LabRAM HR800 system equipped with a 532 nm Nd:YAG laser (Showa Optronics co., Ltd, J100GS-16) and an optical microscope (Olympus, BX41).

X-ray diffraction on whole-rock powders was done to determine bulk sample mineralogy of Darreh Deh lherzolite and to detect the presence of antigorite. The data were obtained using an XRD system (Bruker, D8 Advance, Germany) with a wavelength of 1.5406 Å (Cu Kα), voltage of 40 kV, and current of 40 mA at the Central Laboratory of the University of Isfahan. The XRD patterns confirmed the presence of antigorite, chrysotile, actinolite, clinochlore and forsterite in lherzolite.

4. Data and results

4.1. Petrography and mineral chemistry

The lherzolite is composed of four major primary phases olivine, orthopyroxene, clinopyroxene and Cr-spinel, but later serpentinization and metamorphism resulted in secondary hydrous and non-hydrous Mg-silicate minerals. Lherzolite is composed of olivine (~70 Vol.%) with a forsterite-rich composition (Fo>90%), orthopyroxene (~15-20 Vol.%), clinopyroxene (5-7 Vol.%) and vermicular brown Cr-spinel (<5 Vol.%), together with chlorite, lizardite, chrysotile, talc, tremolite, and metamorphic forsterite (Fig. 2).

Harzburgite and clinopyroxene-bearing harzburgites are characterized by the mineral association olivine (>60-70 Vol.%), orthopyroxene (~30 Vol.%), a small amount of clinopyroxene, sparse subhedral dark brown Cr-spinel (~0.1 mm), talc, tremolite, magnetite and small amounts of chlorite. The rocks show secondary metamorphic textures such as mesh, poikiloblastic, nematoblastic and jack-straw textures, but original magmatic granular and porphyroclastic textures are well preserved. Dunites are composed exclusively of olivine, minor amounts of subhedral, dark brown Cr-spinel, serpentine, metamorphic tremolite, talc and chlorite.

4.1.1. Olivine

In lherzolites, the coarse-grained olivine crystals (<4-5 mm), here named magmatic olivine (Ol_1), formed within the mantle melts, but are not well preserved due to incipient serpentinization (Fig. 2A). Their median magnesium number (Mg# = 100xMg/(Mg+Fe^{2+})) and CaO contents are, respectively, ~90.4 and ~0.034 g/100g (Table 2). In harzburgites, replacive olivine (Ol_r) formed abundantly as reaction rims or within partially corroded orthopyroxene crystals with irregular boundaries (Fig. 2B). Their median Mg# and CaO contents are ~89.4 and ~0.028 g/100g, respectively (Table 2).

4.1.2. Orthopyroxene

Orthopyroxene has kink bands and contains fine exsolution lamellae of clinopyroxene, and resembles primary mantle orthopyroxene. Orthopyroxene is enstatite-bronzite (Mg# = 89.9-90.4) in lherzolite and bronzite (Mg# = 89.2-89.7) in harzburgite (Table 3). As a consequence of magmatic depletion, Al_2O_3 contents (Lhz: ~4.7 g/100g, Hz: ~2.5 g/100g) decrease from lherzolite to harzburgite while TiO_2 (Lhz: ~0.06 g/100g, Hz: ~0.07 g/100g), Cr# = Cr/(Cr+Al) (Lhz: ~0.09, Hz: ~0.17) and Mg# (Lhz: ~91.1, Hz: ~91.6) increase (Table 3).

4.1.3. Clinopyroxene

Clinopyroxenes are diopside-augite in lherzolite and diopside in harzburgite (Table 3); they show kink bands, warped cleavages, and undulatory extinction. The clinopyroxenes in harzburgite have lower Al_2O_3 contents (Lhz: ~5.9 g/100g, Hz: ~3.6 g/100g) and higher TiO_2 (Lhz: ~0.15 g/100g, Hz: ~0.20 g/100g), Mg# (Lhz: ~92.2, Hz: ~93.3) and Cr# (Lhz: ~0.11, Hz: ~0.16) than those in lherzolite (Table 3).

The high field strength (HFSE), heavy (HREE) and light (LREE) rare earth element concentrations of clinopyroxenes from Darreh Deh meta-lherzolite are comparable with those of clinopyroxenes from mantle lherzolite (reported by Pirnia 2007); which for comparison are included in Table 4. Despite similar Mg#, Darreh Deh samples have slightly higher CaO, Rb, Sr and Nb contents but lower Na_2O, NiO, Li, Y, Zr, Ti, Hf and MREE compared to HREE (Table 4). In the chondrite normalized REE diagram (Fig. 4A), clinopyroxenes of Darreh Deh and those reported by Pirnia

(2007) have similar, parallel patterns with flat HREE and MREE and show progressive depletion of LREE (Fig. 4A), but Darreh Deh samples are characterized by slightly higher Eu/Eu* and lower Sm_n/Lu_n (~0.31 for Darreh Deh, ~0.43 for samples from Pirnia 2007) (Table 4). In the primitive mantle normalized diagram (Fig. 4B), the samples show enrichment of HREE above the mantle composition, while other elements (large ion lithophile elements (LILE) and HFSE) are depleted (especially in Darreh Deh samples). The samples are characterized by Zr, Sr and Ba depletion, which is related to magmatic, rather than alteration processes.

4.1.4. Chromian spinel

Vermicular brownish chromian spinels in lherzolite are characterized by having a thin ferrian opaque rim that is occasionally surrounded by a corona of chlorite (Figs. 2C and D). On average, they have Cr#=~0.2, TiO_2 = 0.05 g/100g, Mg# ~76.7, and Al_2O_3 = 48.8 g/100g (Table 5). In harzburgite, Cr-spinels are subhedral dark brownish and one microprobe spinel analysis (Table 5) shows it to be very similar in composition to the Cr-spinels in harzburgites investigated by Pirnia (2007), in being comparatively enriched in Cr# (~0.4) and TiO_2 (~0.22 g/100g), and depleted in Mg# (~53.1) and Al_2O_3 (26.3 g/100g).

4.1.5. Alteration and metamorphic minerals

In addition to magmatic phases (Ol_1 + Opx + Cpx + Cr-Spl), the rocks contain minerals related to alteration and metamorphism. The serpentinization mineral paragenesis in the metamorphosed Darreh Deh lherzolites is Ctl + Lz + Atg, and the metamorphic mineral paragenesis is Tr + Tlc + Chl + Ol_2.

Metamorphic olivines (Ol_2) recrystallized as fine-grained (<0.1mm) neoblasts at the expense of serpentines. Magmatic, replacive, and metamorphic olivines all have approximately similar major elements contents; however, the median CaO of the metamorphic olivines (Ol_2) is lower (~0.012 g/100g), and the Mg# of Ol_2 has not the same range as Ol_1 due to partial increment of Fe^{2+}/Mg in some Ol_2 (Table 2, Fig. 3).

Tremolite is the other abundant metamorphic phase in the metamorphosed peridotites of Darreh Deh. The Ca-bearing tremolite to tremolitic hornblende (Table 6) developed as nematoblastic and jack-straw textures in cracks within and/or around clinopyroxene (Fig. 2C) and basititized orthopyroxene porphyroclasts in lherzolite (Fig. 2E). According to Khedr & Arai (2012) and Nozaka (2014), these tremolites can be categorized into partially-retrograde (Tr_1) and prograde (Tr_2) tremolite. The fibrous crystals of retrograde tremolite (Tr_1) are tremolitic hornblende in composition with higher Al_2O_3 (~4.3 g/100g), Cr_2O_3 (~0.8 g/100g), Na_2O (~0.7 g/100g), and lower SiO_2 (~53.8 g/100g), whereas acicular crystals of prograde tremolite have lower Al_2O_3 (~2.4 g/100g), Cr_2O_3 (~0.4 g/100g), Na_2O (~0.4 g/100g), and higher SiO_2 (~55.7 g/100g) contents (Table 6). The retrograde tremolitic hornblende (Tr_1) formed at the expense of clinopyroxene, and was afterwards replaced by tremolite (Tr_2). The higher Cr content of Tr_1 was inherited from its clinopyroxene source. Tremolite is a prograde product after talc (Fig. 2E), chrysotile (Fig. 2F) and chlorite (Fig. 2G), wherever the associated olivine (or orthopyroxene) has been serpentinized and the Ca^{2+} ions released to contribute to the tremolite structure. XRD patterns also confirm the occurrence of minor amounts of actinolite in the lherzolite (Fig. 5). In metamorphosed harzburgite samples, tremolite has replaced formerly serpentinized pyroxene crystals or occurs as thin needles or sheaves of needles penetrating neighboring olivines. Tremolite also formed in the metamorphosed dunites after olivine serpentinization.

Fig. 2. Photomicrographs of Darreh Deh metamorphosed peridotites (Nain Ophiolite): (A) Metamorphic fine-grained olivine neoblasts (Ol_2) together with magmatic olivine (Ol_1) containing serpentine veins; (B) Orthopyroxene containing minute clinopyroxene crystals as exsolutions, and having irregular and partially corroded boundaries in which replacive olivine have formed by incongruent melting of orthopyroxene (Ol_r = replacive olivine); (C) Crossed nicols and (D) Plane-polarized light images of vermicular brownish chromian spinel with magnetite at the rims, and chlorite alteration rims. Clinopyroxene rims are replaced by tremolite. Upper right shows serpentine veins crossing Ol_1, but not Ol_2; (E) Orthopyroxene altered to and surrounded by nematoblastic and jack-straw textured talc and tremolite (crossed nicols); (F) A bastized orthopyroxene replaced by chrysotile (Ctl). The chrysotile is substituted by lizardite (Lz) and reacting to tremolite (Tr); (G) Tremolite needles formed in a chloritized matrix; (H) Olivine altered and surrounded by nematoblastic and jack-straw textured talc and tremolite (crossed nicols).

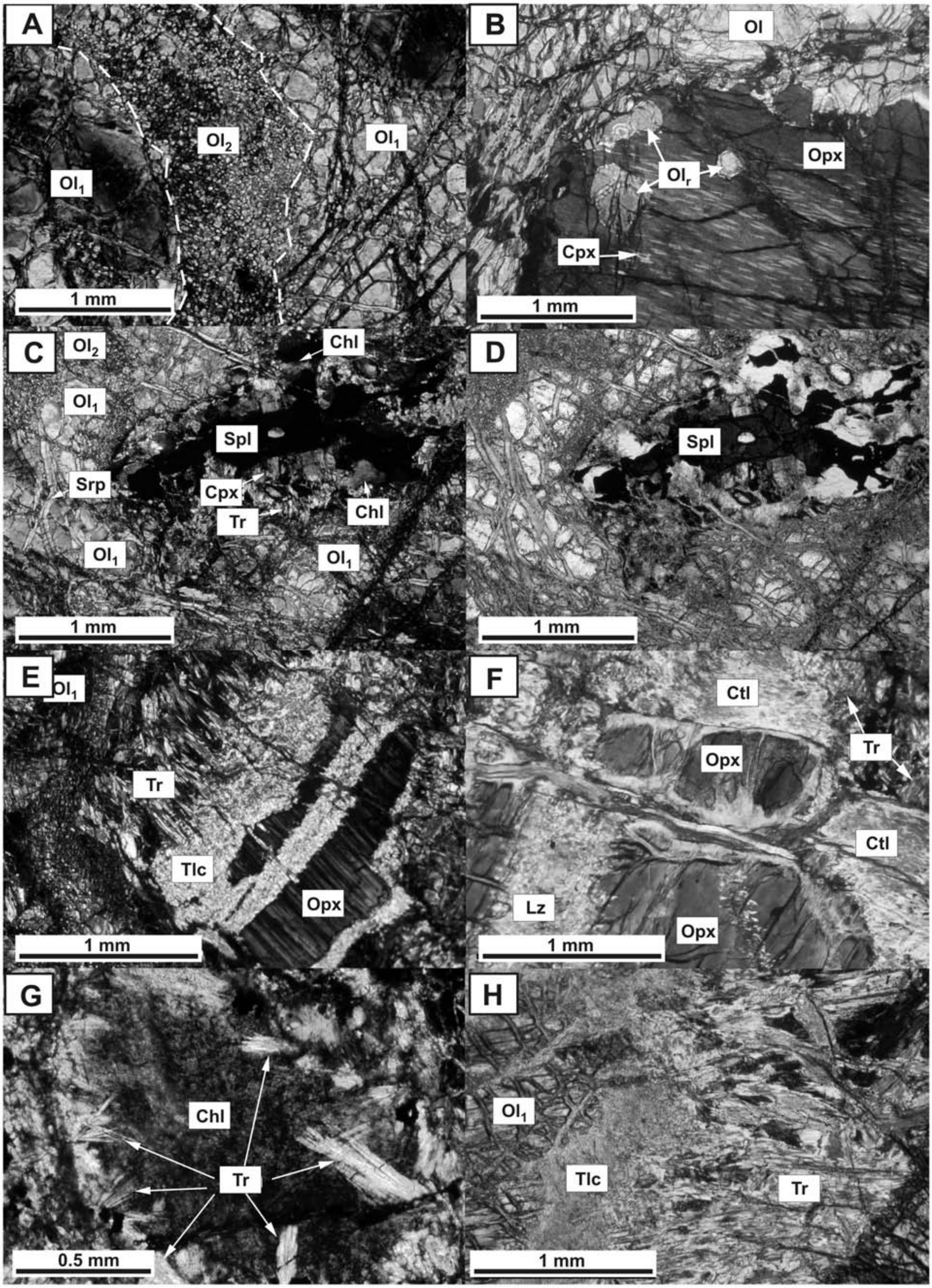
A
Ol_2
Ol_1
Ol_1
1 mm
B
Ol
Opx
Ol_r
Cpx
1 mm
C
Ol_2
Chl
Ol_1
Spl
Srp
Cpx
Tr
Chl
Ol_1
Ol_1
1 mm
D
Spl
1 mm
E
Ol_1
Tr
Tlc
Opx
1 mm
F
Ctl
Tr
Opx
Ctl
Lz
Opx
1 mm
G
Chl
Tr
0.5 mm
H
Ol_1
Tlc
Tr
1 mm

Fig. 2.

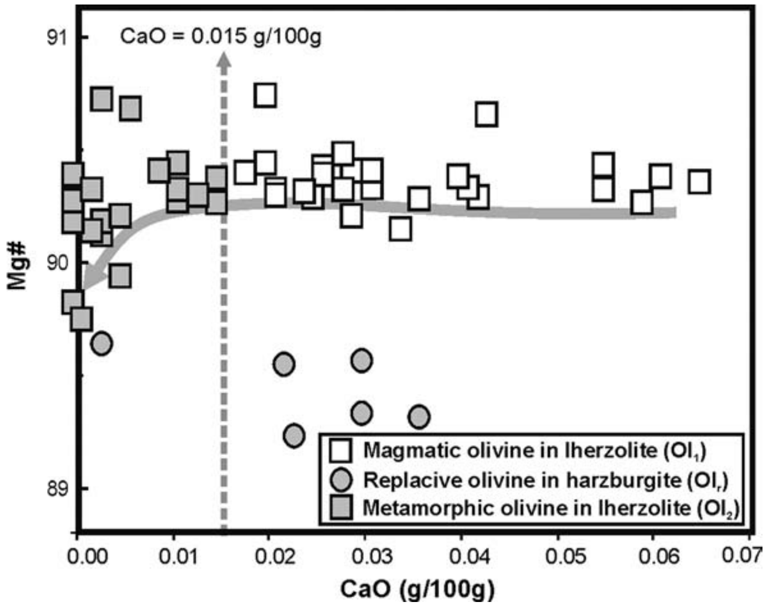

Fig. 3. CaO versus Mg# (in g/100g) diagram for magmatic (Ol_1), replacive (Ol_r), and metamorphic olivine (Ol_2) in metamorphosed mantle peridotites of Darreh Deh massif.

Talc is a common product of low-grade metamorphism and formed along the cleavages of orthopyroxene or olivine, and was progressively metamorphosed into tremolite wherever a serpentinized orthopyroxene or olivine was associated (Figs. 2E and H).

Raman spectrometry of serpentine minerals indicates that the mesh texture is made of lizardite whereas the crosscutting serpentine-filled veins (V_1) are chrysotile. In addition, XRD analysis proved the presence of antigorite in some lherzolite samples (Fig. 4). It is difficult to identify the antigorite in thin section but formation of secondary olivines (mostly in the veins) reveals that antigorite formation was limited to the veins.

Chrysotile veins (V_1) cut all primary phases (e.g. olivine, pyroxene porphyroclasts, and lizardite) but not the metamorphic phases (e.g. olivine neoblasts (Ol_2), tremolite, talc and chlorite) (Fig. 2C). Lizardite with high Mg, Fe and Ni contents (Table 6) replaced olivine, while the low Mg and high Cr contents of Al-rich serpentine (chrysotile) in orthopyroxene bastite reflect the composition of the original orthopyroxene (Dungan 1979, Wicks & Plant 1979, in Shervais et al. 2005).

Some serpentines reacted to form chlorite, indicating that chloritization followed serpentinization. The XRD pattern indicates that clinochlore may be present in lherzolite as well (Fig. 4). Chlorite also occurs as veins (V_2) crosscutting the older V_1 serpentine veins. Some chlorites (clinochlore) are in the rim of Cr-spinel and some (talc-chlorite) formed at the expense of clinopyroxenes, however, they are mostly replaced by tremolite during prograde metamorphism (Table 6).

4.2. Bulk rock composition

The chemical data for selected metamorphosed Darreh Deh peridotites are given in Table 7, for comparison together with published data for peridotite samples from the central parts of the Nain Ophiolite (taken from Ghazi et al. 2011; Torabi 2013). Darreh Deh peridotites are characterized by slightly higher SiO_2, Na_2O, Sc, V, Cr and heavy REE contents and lower loss of ignition (LOI) values. The CaO, Al_2O_3 and HREE contents of lherzolites positively correlate with clinopyroxene abundance. CaO/Al_2O_3 reflecting clinopyroxene content is higher in lherzolites (~1.01-1.57) than in harzburgite (~1.05-1.28) and dunite (~0.81-0.90). Darreh Deh peridotites are characterized by LOI values between ~7 and 10 g/100g. LOI cannot be used as a criterion for degree of serpentinization (Deschamps et al. 2013), but samples have Al_2O_3, CaO, MgO, Ni and Cr content comparable to less, or not, serpentinized residual mantle peridotites (e.g. Taylor & McLennan 1985; Bodinier et al. 1988). It seems that

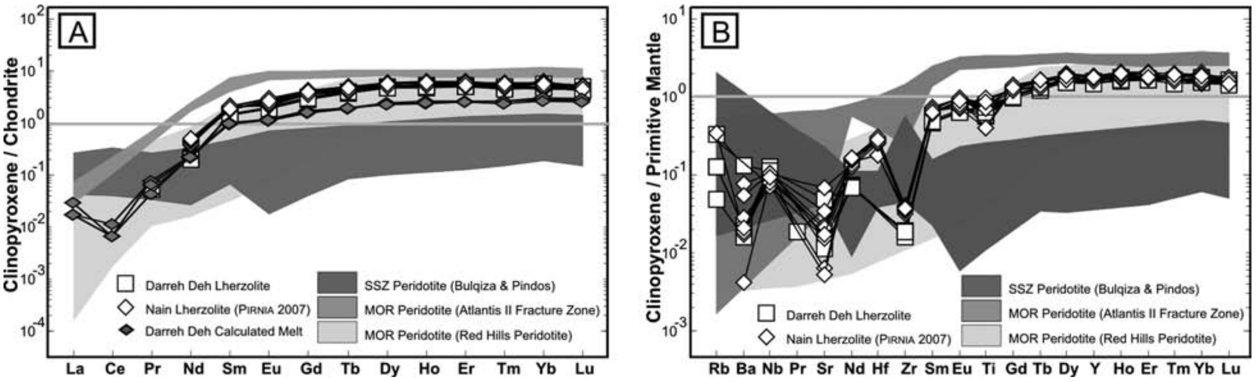

Fig. 4. (A) Chondrite-normalized analyses of clinopyroxene (in lherzolite) and calculated melt for Darreh Deh samples and published data from Pirnia (2007) (Table 4); (B) Primitive mantle normalized composition of clinopyroxene in Darreh Deh lherzolite and published data from Pirnia (2007). The fields are clinopyroxene composition data of MOR peridotites from the Red Hills peridotite in the Dun Mountain ophiolite of South Island, New Zealand (Sano & Kimura 2007) and the Atlantis II Fracture Zone (Johnson & Dick 1992), and SSZ peridotites of the Hellenic Peninsula, Pindos, and Bulqiza in Albania (Bizimis et al. 2000). Chondrite and primitive mantle normalization factors are from McDonough & Sun (1995).

serpentinization can increase the CaO of bulk rock dunite (e.g. Fig. 3d in Deschamps et al. 2013), possibly due to olivine decomposition (See section 2.a). In addition, Al, Ca, Cr, Zn, Y, Sc, V, Ga and HREE contents decrease from lherzolite to harzburgite and dunite, whereas Mg#, MgO, Ni, Co, and some of the light rare earth elements increase (Table 7).

Fig. 6 shows chondrite and primitive mantle normalized bulk-rock REE and trace element abundances of Darreh Deh metamorphosed peridotites. Darreh Deh peridotites have compositions and REE patterns that are similar to peridotites from the central parts of the Nain Ophiolite (e.g. Ghazi et al. 2011; Torabi 2013). Harzburgite and dunite show a slightly flat chondrite-normalized REE patterns while lherzolites are HREE-enriched (Fig. 6). The peridotites are characterized by increasing normalized LREE to HREE contents, while La_n/Yb_n, La_n/Sm_n and Gd_n/Yb_n ratios in Darreh Deh samples constantly increase from lherzolite to harzburgite and dunite (Table 7). Eu shows a weak positive anomaly (Eu/Eu* ~1.2-1.7) as is common in the most depleted and primitive MORB melts due to late crystallization of plagioclase, serpentinization, or seafloor weathering (Niu 2004).

On the primitive mantle normalized diagram (Fig. 6E), Rb, Ba, Pb and Sr are more enriched and have similar values as primitive mantle. Co, Sc, V, Ga are more or less immobile or unaffected by serpentinization and seafloor weathering (e.g. Niu 2004 & references therein).

5. Discussion

5.1. Metamorphic events

The P-T pseudosection modeling of a lherzolite sample was performed using the Perple X software (Connolly 1990) and the hp02ver.dat file containing the thermodynamic data set of Holland & Powell (1998). The chemical system considered in the P-T pseudosection is CFMASH (sample L-223-2) (Fig. 7). This diagram yields the possible mineral assemblages in the sample in the considered P-T range of 1-30 kbar and 300-1000 °C. In the following we explain how Darreh Deh peridotites, petrographic relics and chemical evidence indicate a greenschist-facies stage (serpentinization and chloritization) that was followed and overprinted by a prograde amphibolite-facies metamorphic stage.

5.1.1. Early greenschist-facies stage (serpentinization and chloritization)

Some ultrabasic bodies in ophiolites were probably serpentinized in an oceanic setting prior to the regional metamorphism, and the serpentinization stage in Darreh Deh peridotites be related to serpentinization in a fast mid ocean rifting system. The slightly lower degree of serpentinization of harzburgite and dunite compared to lherzolite indicates that serpentinization occurred by fluid infiltration before and during melt-rock interaction in a rift to intra-oceanic subduction setting. In comparison with serpentinized peridotites

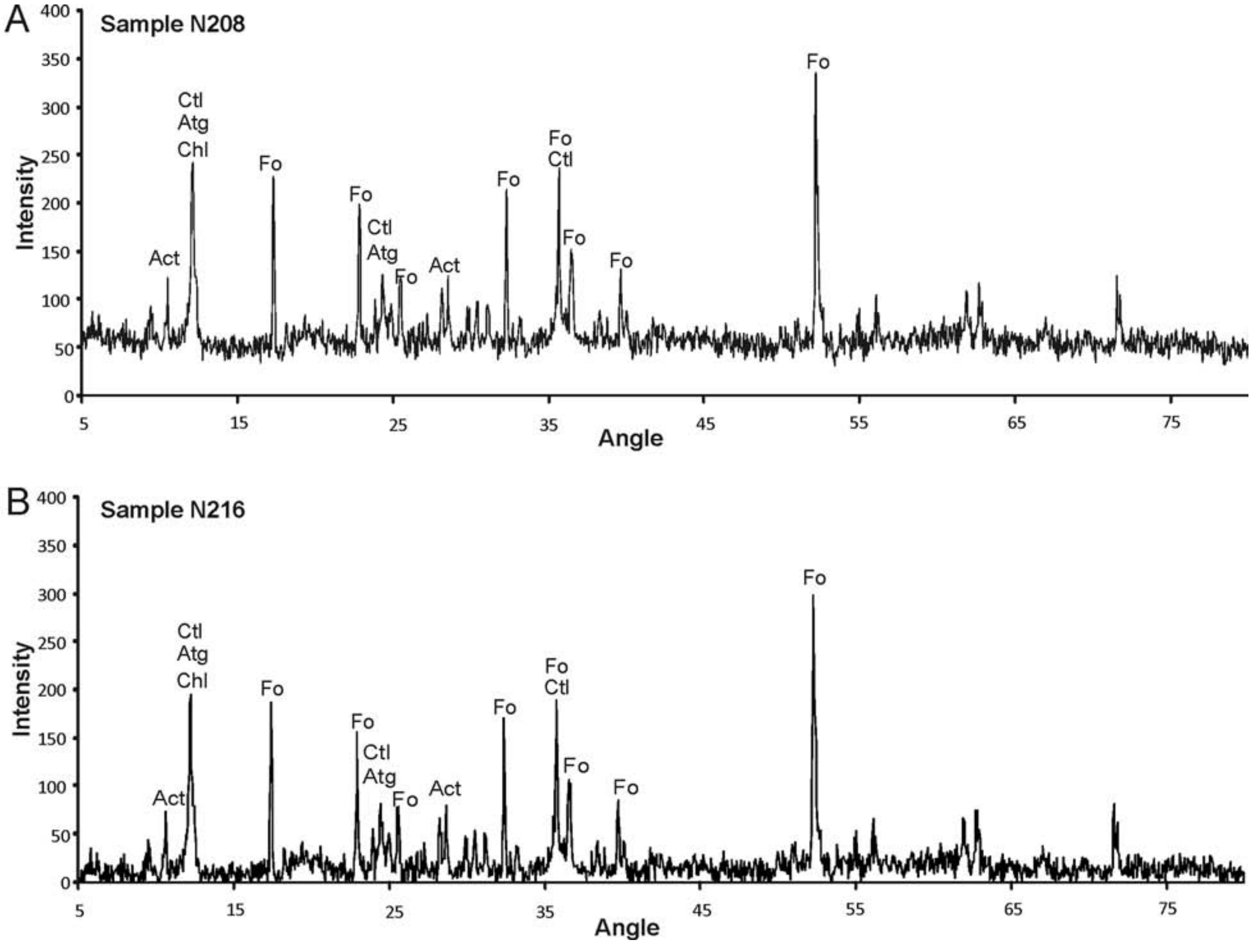

Fig. 5. (A) and (B) Whole rock XRD pattern for Darreh Deh lherzolite (Act = actinolite, Atg = antigorite, Fo = forsterite, Chl = clinochlore, Ctl = chrysotile).

from other settings (e.g. Deschamps et al. 2013, and references therein), Darreh Deh lherzolites are more comparable with forearc or “mantle wedge” serpentinites (e.g. Guillot et al. 2009; Deschamps et al. 2013) and Darreh Deh harzburgite and dunite partly differ from subducted serpentinites (e.g. Deschamps et al. 2013). However, Darreh Deh lherzolite, harzburgite and dunite compositions show low contrasts in trace element contents (except for the higher MREE and HREE in lherzolites) due to their lower serpentinization degrees compared to the samples of Deschamps et al. (2013). Therefore, it is very difficult to assign the serpentinization to a certain geological setting on the basis of published serpentinization studies (e.g. Deschamps et al. 2013), and more research is needed.

The non-pervasive serpentinization is delineated by serpentine relics found mostly around the ferromagnesian minerals olivine and pyroxene, or filling crosscutting veins. This low-temperature serpentinization stage is a result of chemical interaction with seawater, which resulted in early replacement of olivine (Ol_1) by lizardite (forming a mesh texture) and chrysotile (in crosscutting V_1 veins), and the formation of chrysotile at the expense of orthopyroxene in lherzolite. Serpentinization can release Ca^{2+} cations from primary phases. For example, primary olivines (Ol_1) in Darreh Deh lherzolite contain >0.015 g/100 g CaO (in the M_2 site), and this CaO was involved in the crystallization of Ca-bearing minerals (e.g. tremolitization, rodingitization). Evans (2004) and Lafay et al. (2013) suggested formation temperatures of 50-300 °C for vein chrysotile, and 0-400 °C for the lizardite in the bastite/mesh texture (by hydration of peridotites). Lizardite and chrysotile are progressively replaced by antigorite at 320-390 °C (Schwartz et al. 2013) or from 300 to 650 °C (Evans 2004; Lafay et al. 2013). The reaction

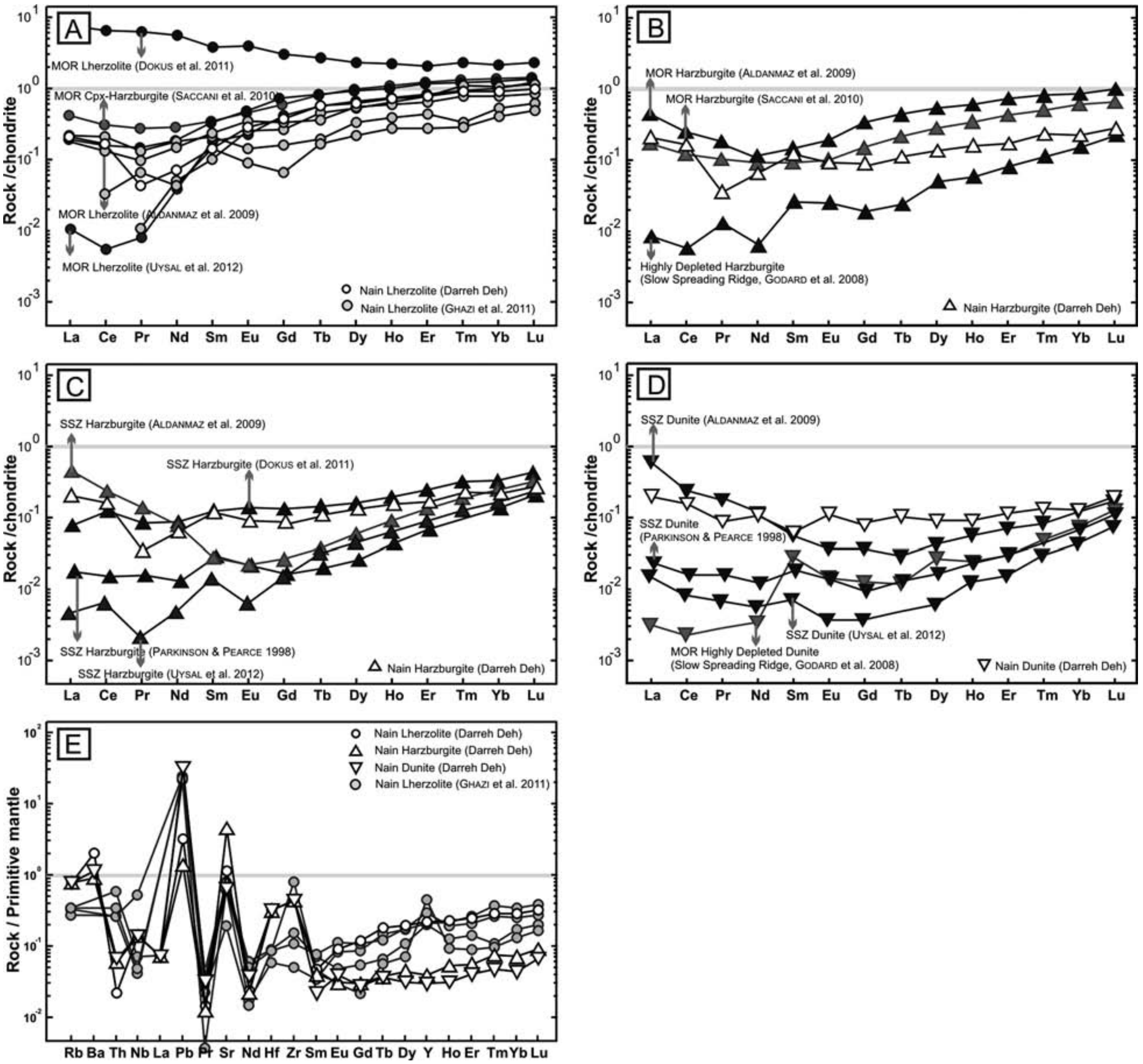

Fig. 6. (A) Chondrite-normalized compositions of Darreh Deh mantle lherzolite and published data from Ghazi et al. (2011), compared to MOR lherzolite and Cpx-harzburgite data are from Aldanmaz et al. (2009), Saccani et al. (2010), Dokus et al. (2011), and Uysal et al. (2012); (B) Chondrite-normalized compositions of Darreh Deh harzburgite, compared to MOR harzburgite data from Godard et al. (2008), Aldanmaz et al. (2009), and Saccani et al. (2010); (C) Chondrite-normalized compositions of Darreh Deh harzburgite, compared to SSZ harzburgite data from Parkinson & Pearce (1998), Aldanmaz et al. (2009), Dokus et al. (2011), and Uysal et al. (2012); (D) Chondrite-normalized compositions of Darreh Deh dunite, compared to SSZ and MOR dunite data from Parkinson & Pearce (1998), Godard et al. (2008), Aldanmaz et al. (2009), and Uysal et al. (2012); (E) Primitive mantle normalized compositions of Darreh Deh mantle peridotites. Chondrite and primitive mantle normalization factors are from McDonough & Sun (1995).

$$2Mg_3Si_2O_5(OH)_4 + H_2O \rightarrow Mg_3Si_2O_5(OH)_4 + 3Mg(OH)_2 + 2SiO_2$$

shows chrysotile stability and its conversion to antigorite. The P-T pseudosection modeling indicates ~500 to 700 °C/1 to 30 kbar as the upper P-T stability limit for antigorite in the lherzolite sample. The progressive replacement of chrysotile + lizardite assemblages by antigorite + lizardite indicates the prograde greenschist-facies metamorphism (Bliss & MacLean 1975).

The chloritization occurred after serpentinization because chlorite-filled V$_2$ veins crosscut the chrysotile-filled V$_1$ veins. P-T pseudosection modeling (Fig. 7) indicates ~650 to 850 °C at 1 to 30 kbar as the upper possible P-T stability limit for chlorite (clinochlore) that formed after Cr-spinel in the metamorphosed lherzolite sample. Thus, the chloritization of Cr-spinels occurred during serpentinization and continued during regional metamorphism.

5.1.2. Later amphibolite-facies stage

The Darreh Deh peridotites preserved petrographic evidence for a prograde stage of metamorphism, characterized by the formation of antigorite after lizardite and chrysotile, metamorphic olivine neoblasts (Ol$_2$) after serpentines, clinochlore after Cr-spinel, talc after olivine, and orthopyroxene and tremolite after pyroxene and talc, serpentine, and chlorite. The evidence is discussed below. This prograde metamorphism has occurred after melt-rock interactions because it also overprinted harzburgites and dunite.

The early grade of metamorphism of this stage reached the upper stability limit of antigorite, which is known to be stable over a temperature range of 300-650 °C and formed at the onset of prograde metamorphism, close to where tremolite appeared (Fig. 7). Schwartz et al. (2013) suggested a temperature of 460 °C for the onset of secondary olivine crystallization. The fine-grained secondary olivines (<0.1 mm) found in the present study are very similar to the minute grains of secondary metamorphic olivines (~50 μm) in antigorite veins reported by Debret et al. (2013).

The reaction sequence olivine (Ol$_1$) → lizardite → chrysotile → olivine (Ol$_2$) ± talc (Hayakawa et al. 2006) shows that chrysotile may dehydrate and decompose into a metastable assemblage of forsterite + talc. In the pure MgO-SiO$_2$-H$_2$O system, antigorite can also react to produce secondary olivine + talc at ~515 °C and 2 kbar (Evans et al. 1976). In the CFMASH phase diagram (Fig. 7) within the tremolite P-T stability field, antigorite reacts to form talc at ~540 to 700 °C. The reaction antigorite → talc + olivine (Ol$_2$) + chlorite+H$_2$O (Worden et al. 1991) may best describe the formation of olivine neoblasts from antigorite.

The compositions of olivine and other minerals are supposed to be controlled by bulk-rock chemistry and metamorphic grade (Torabi et al. 2011a). For example, the magmatic olivine (Ol$_1$) having crystallized in the mantle, has higher CaO contents of > 0.015 g/100g (or Ca > 0.010 g/100g), while metamorphic olivine neoblasts (Ol$_2$) are comparatively Ca-poor to Ca-free (CaO <0.015 g/100g) (Fig. 3). Comparable results can be found in the LA-ICP-MS data in Table 3 of Debret et al. (2013) for the magmatic (Ca ~0.028 g/100g) and secondary olivines (Ca ~ 0.016 g/100g). Calcium partitioning in olivine is temperature dependent (e.g. Hoog et al. 2010) and, hence, is higher in mantle olivines compared to olivines formed by metamorphism. In addition, the lower Ca content of olivine neoblasts (Ol$_2$) is due to their recrystallization after low calcium serpentine:

$$\mathrm{Ol}_{1(\mathrm{CaO}>0.015\ \mathrm{g/100g})} \rightarrow \mathrm{Serpentine}_{(\mathrm{CaO}<0.01\ \mathrm{g/100g})} + \mathrm{Ca}^{2+} \rightarrow \mathrm{Ol}_{2(\mathrm{CaO}<0.015\ \mathrm{g/100g})} + \mathrm{Ca}^{2+}$$

The reactions that describe the release of Ca^{2+} from orthopyroxene and olivine during serpentinization are:

$$3(\mathrm{Mg, Ca}_{<0.1})_2\mathrm{Si}_2\mathrm{O}_6 + 4\mathrm{H}_2\mathrm{O} \rightarrow 2\mathrm{Mg}_3\mathrm{Si}_2\mathrm{O}_5(\mathrm{OH})_4 + 2\mathrm{SiO}_2 + \mathrm{Ca}^{2+}$$

$$3(\mathrm{Mg, Ca}_{\sim 0.001})_2\mathrm{SiO}_4 + \mathrm{SiO}_{2(aq)} + 2\mathrm{H}_2\mathrm{O} \rightarrow 2\mathrm{Mg}_3\mathrm{Si}_2\mathrm{O}_5(\mathrm{OH})_4 + \mathrm{Ca}^{2+}$$

Ca^{2+} released during serpentinization of olivine and pyroxene cannot be accommodated in the serpentine, talc and olivine lattice. As a consequence, the olivine neoblasts (Ol$_2$) that formed by serpentine-consuming reactions are depleted in Ca^{2+} (CaO<0.015 g/100g, Table 2).

In addition, the Mg# of metamorphic olivines has not the same range as that of Ol$_1$ (it is ~0.2 lower in some Ol$_2$). Lower Fe^{2+}/Mg in some Ol$_2$ analyses is due to low Fe^{2+} partitioning into serpentines and concentration of Fe, mostly in fine-grained aggregates of magnetite (e.g. Niu 2004). Moreover, even at low Fe contents the octahedral M$_2$ site of orthopyroxene prefers calcium above ferrous iron (Rietmeijer 1983). Müntener et al. (2000) indicated that orthopyroxene in ultramafic rocks may break down by hydration to olivine + tremolite + chlorite + talc at ~600 (±50) °C and ~10 kbar.

The calcic amphibole in high-grade metaperidotite (at amphibolite facies), tremolite, is stable at 550-800 °C along the kyanite geotherm in the pure MgO-SiO$_2$-H$_2$O system (Bucher & Frey 2002). In our samples, it mostly progressively developed around clinopyroxene and orthopyroxene, chloritized clinopyroxene, chrysotile around orthopyroxene, and serpentinized or metamorphic olivine (Ol$_2$). In the CFMASH system, it is stable over the temperature range 550 to 850 °C, i.e. amphibolite to granulite facies (Fig. 7). According to Spear (1995), those tremolites with 7.4<Si<7.9 a.p.f.u.,

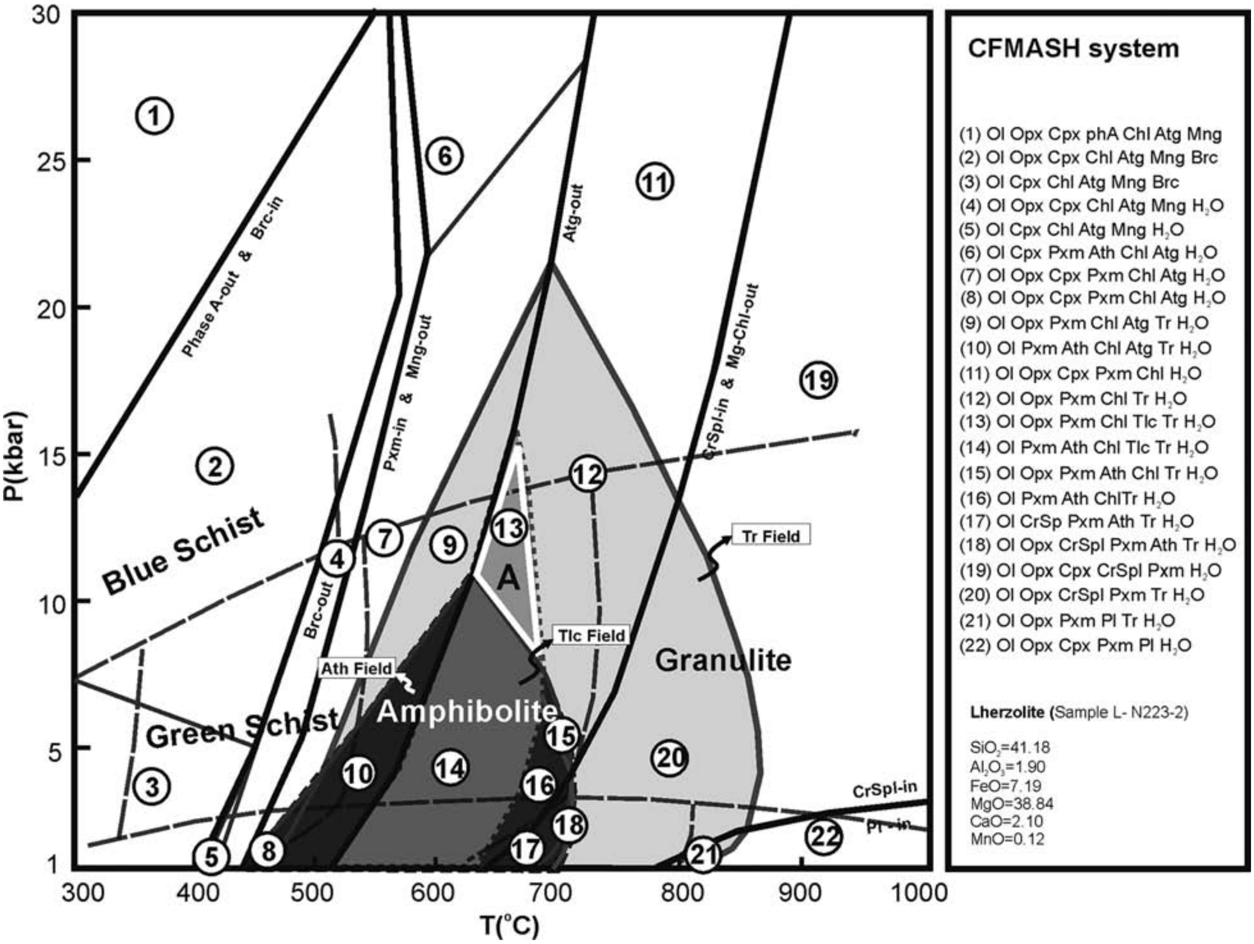

Fig. 7. P-T Pseudosection (CFMASH system) calculated for Darreh Deh metamorphosed lherzolite (sample L-223-2, Table 7). Mineral abbreviations are from WHITNEY & EVANS (2010).

together with associated forsterite and talc, constitute the characteristic medium amphibolite-facies assemblage in the Darreh Deh metaperidotites.

Spinel in Darreh Deh metaperidotites is replace by Mg-rich clinochlore and talc-chlorite assemblages that are stable at amphibolite- to granulite-facies conditions (~550-800 °C and <15 kbar) (Fig. 7). In addition to serpentinization of magmatic olivine Ol_1 and orthopyroxene; chloritization of clinopyroxene provided another Ca^{2+} source for tremolite formation (Figs. 2C, E and F):

$$\text{Clinopyroxene}_{(CaO\sim 20\ g/100g)} \rightarrow \text{Chlorite}_{(CaO<0.02\ g/100g)} + Ca^{2+}_{(out)} \rightarrow \text{Tremolite}_{(CaO\sim 12\ g/100g)}$$

$$2.5(Mg, Ca\sim 0.0 \text{ to } <0.1)_2Si_2O_6 + 3SiO_{2(aq)} + H_2O + 2Ca^{2+} \rightarrow Ca_2Mg_5Si_8O_{22}(OH)_2$$

Although harzburgite and dunite have lower CaO contents due to the smaller amounts of clinopyroxene, they still contain tremolite as a metamorphic product, which confirms that enough Ca^{2+} was released from olivines after serpentinization.

According to SHIRDASHTZADEH et al. (2010, 2011), amphibolites are found within the mantle peridotites in the shape of metamorphosed basic pillow lavas and basic feeder and diabasic dikes. For amphibolites of the Nain Ophiolite, SHIRDASHTZADEH et al. (2010) reported that Jurassic-age high-grade metamorphism occurred at temperatures and pressures of 650-800 °C and 7-8 kbar (upper amphibolite to lower granulite facies). Judging from the CFMASH pseudosection these temperatures overlap the estimated P-T range for the common mineral assemblages of Darreh Deh metamorphosed mantle lherzolite. The observed mineral assemblage olivine + clinopyroxene + orthopyroxene + chromian spinel + antigorite + metamorphic olivines (after deserpentinization of serpentines) + talc + tremolite + chlorite could have formed at amphibolite-facies conditions at approximately 630-700 °C and 7-15 kbar (Field A, Fig. 7).

5.2. Petrogenesis of Darreh Deh mantle peridotites

According to Deschamps et al. (2013), REE abundances can be used to identify the protolith of serpentinized peridotites (e.g. abyssal and mantle wedge serpentinized lherzolite, harzburgite and dunite) and identify later magmatic processes. For example, LREE enrichment in subducted serpentinized peridotites could be related to magmatic processes before serpentinization (such as melt/rock interactions and/or the intrinsic nature of the protolith) or after serpentinization (such as the magmatic refertilization process during the sedimentary derived fluid/rock interactions within the subduction channel).

Although hydration and dehydration during serpentinization, metamorphism, and shearing may alter the compositions of the primary minerals of a peridotite to some extent, the compositions of relict minerals (i.e. clinopyroxene and chromian spinel) together with the bulk rock composition can be used to constrain the mantle processes involved in peridotite formation.

5.2.1. Bulk rock composition

MgO decrease in peridotites can be a result of partial alteration of olivines and pyroxenes to serpentines (e.g. Snow & Dick 1995; Bach et al. 2004; Niu 2004; Paulick et al. 2006). However, the inverse correlation of MgO with progressively heavier rare earth elements reflects varying degrees of melt depletion and post-melting magmatic refertilization (Niu 2004). For Darreh Deh lherzolite to harzburgite and dunite, Al_2O_3 and Cr decrease with increasing Mg#, as is the case for the samples from the central parts of the Nain Ophiolite (i.e. Torabi 2013, Ghazi et al. 2011) (Table 8). Such a trend is explained by melt-rock interaction, rather than depletion of a fertile mantle lherzolite by extraction of a basaltic component during high degrees of partial melting.

The REE pattern reveals a complex series of events for the oceanic crust of the Nain Ophiolite. The chondrite-normalized REE patterns of harzburgite and dunite are flatter than those of lherzolite (Fig. 6A, B and D). It is possible to interpret this pattern as reflecting REE depletion (particularly LREE), but also HREE enrichment at a later stage. Initial partial melting of lherzolite and incremental consumption of clinopyroxene resulted in decreasing clinopyroxene/orthopyroxene ratios in residual lherzolite. The ascending melts reacted with the lherzolitic wall rocks causing incongruent orthopyroxene melting. While being depleted in clinopyroxene, modal amounts of olivine (Ol_r) replacing orthopyroxene gradually increased to form replacive harzburgite and finally dunite. As consequence of such melt-rock reaction, the lower clinopyroxene/orthopyroxene ratio resulted in flatter REE patterns in harzburgite and dunite (Fig. 6B and D).

In Fig. 6, Darreh Deh peridotites are compared to the average composition of some worldwide examples of MOR and SSZ peridotites. On the chondrite-normalized REE pattern, MOR lherzolites show a wide range of REE abundances, particularly for the LREE. For example, the samples from Dokuz et al. (2011) are more REE-enriched, and samples from Uysal et al. (2012) are more depleted in LREE. Darreh Deh lherzolite is very similar to the lherzolite and clinopyroxene-harzburgite samples from the Nehbandan ophiolitic complex (eastern Iran) (Saccani et al. 2010) and mid-ocean ridge lherzolites from Neo-Tethyan ophiolites in SW Turkey (Aldanmaz et al. 2009) (Fig. 6A).

Darreh Deh harzburgites have flatter REE patterns that show some similarity with the MOR harzburgites from the Neo-Tethyan ophiolites in SW Turkey (Aldanmaz et al. 2009) and the Nehbandan ophiolitic complex (Saccani et al. 2010), especially in the more mobile LREE contents, while the less mobile HREE have slightly lower concentrations (Fig. 6B). The MOR harzburgite of Godard et al. (2008), drilled at ODP Sites 1272 and 1274 (Fifteen-Twenty Fracture Zone, slow spreading Mid-Atlantic Ridge), is the most HREE depleted. In Fig. 6C, the Darreh Deh samples REE patterns that very similar to SSZ harzburgite from Dokuz et al. (2011), and HREE abundances similar to those of Aldanmaz et al. (2009) and Parkinson & Pearce (1998). The MREE and LREE, however, show a wide range of abundances. The REE concentrations of SSZ dunites vary widely, but those of the Darreh Deh dunite are similar to the SSZ dunites of Aldanmaz et al. (2009). In fact, the REE content of MOR lherzolite is higher than that of MOR and SSZ harzburgite, and the

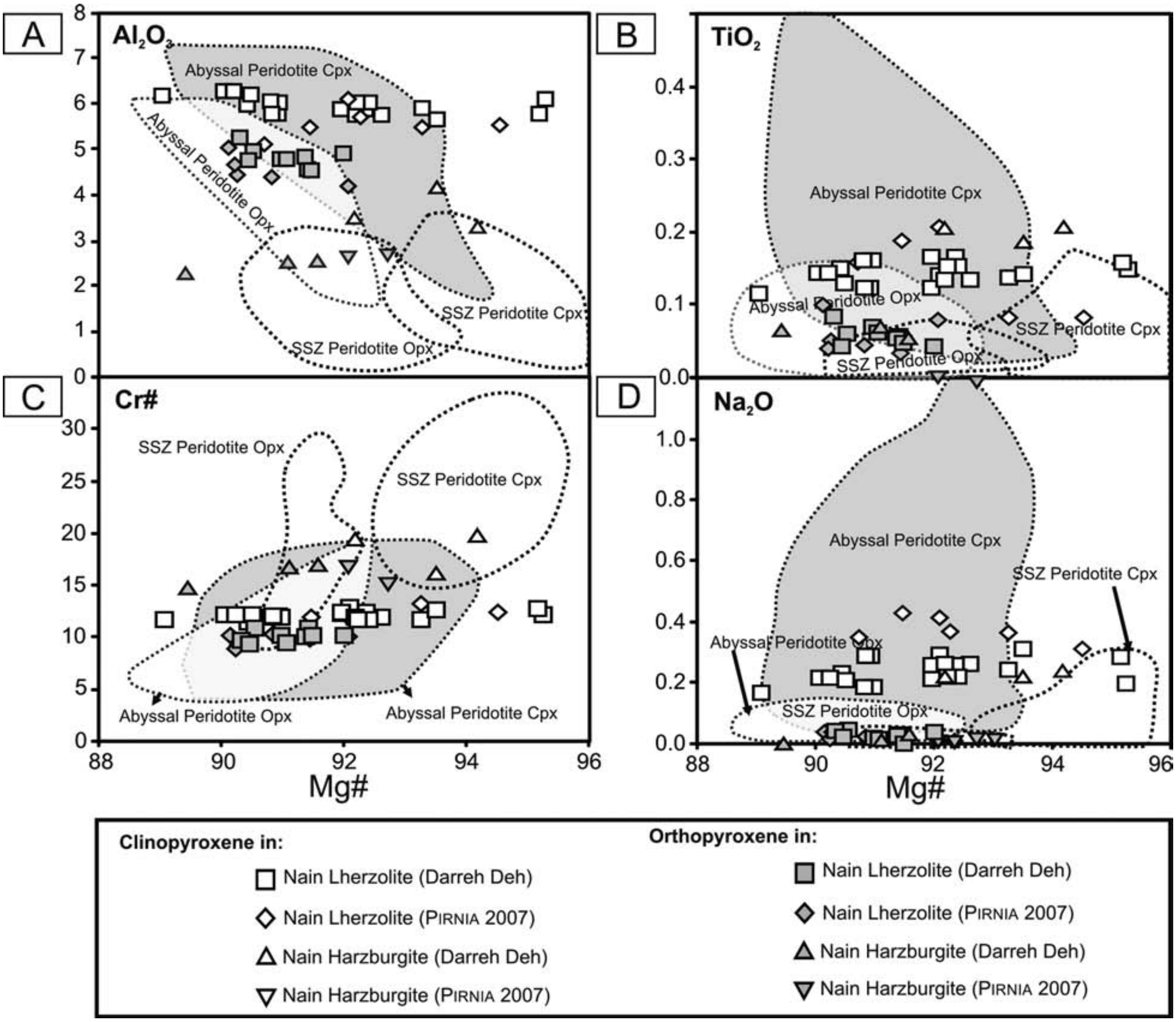

Fig. 8. Composition of clino- and orthopyroxene from lherzolite and harzburgite of the Nain Ophiolite: (A), (B), (C) and (D) Mg# versus Al_2O_3, TiO_2, Cr# and Na_2O (in g/100g). The MOR and SSZ fields are from Aldanmaz (2012). The fields are from the Coast Range ophiolite (CRO) of California in North American Cordillera (Choi et al. 2008 & references therein).

REE content of dunite is the lowest. However, due to their overlapping ranges of REE abundance it is difficult to characterize a MOR or SSZ origin for the harzburgites based on REE patterns alone. Therefore, bulk harzburgite REE data are unspecific because magmatic processes in SSZ harzburgite may have taken place at different rates (e.g. melt-rock reactions), depending on the sinking slab, the released fluids, and the mantle wedge partial melting.

The progressive decrease of LREE and MREE concentrations from Darreh Deh lherzolite to harzburgite and dunite indicates a SSZ tectonic setting in which, for example, an intra-oceanic arc formed above a subduction zone. Subduction of oceanic lithosphere and sediments into the mantle beneath the pre-existing mid-ocean ridge lithosphere caused modification of the mantle by hydrous fluids and melts that were derived from the dehydration of the sinking slab, resulting in a nascent supra-subduction zone magmatic system.

On the primitive mantle normalized diagram, enrichment of the fluid mobile elements Sr, Pb, U, Rb and Ba (Fig. 6E) is similar for serpentinized peridotites (e.g. Sulabest ophiolite (Eastern Iran), Angiboust et al. 2013; Deschamps et al. 2013; Debret et al. 2013),

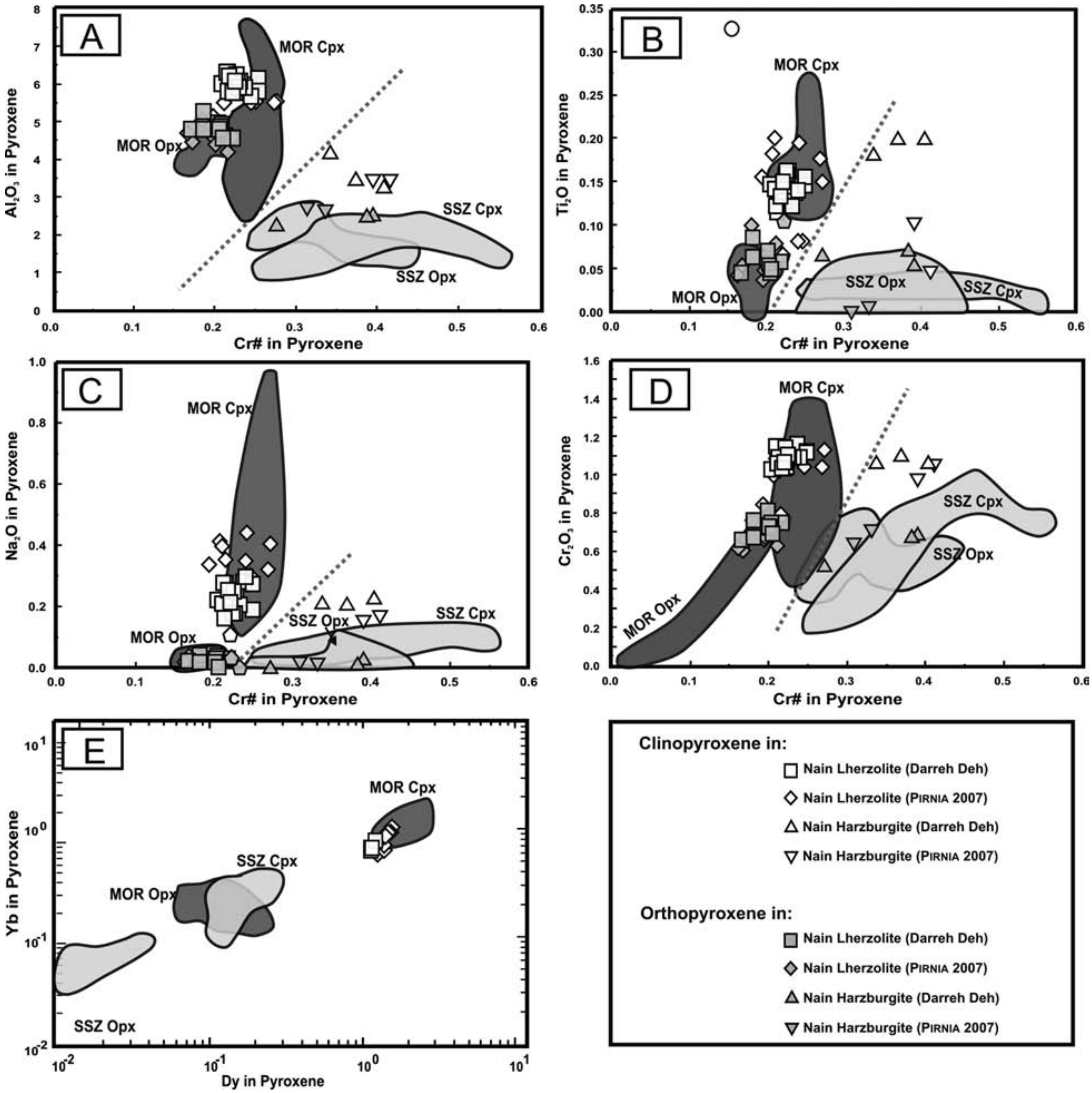

Fig. 9. Composition of clinopyroxene and orthopyroxene from lherzolite and harzburgite of the Nain Ophiolite: (A), (B), (C) and (D) Cr# versus Al$_2$O$_3$, TiO$_2$, Na$_2$O and Cr$_2$O$_3$ (in g/100g) (=Cr/Cr+Al^{vi}); (E) Yb versus Dy (in μg/g). The MOR and SSZ fields are from Aldanmaz (2012). Major element oxides are in g/100g and trace elements are in μg/g.

including examples of less serpentinized MOR and SSZ peridotite (e.g. Godard et al. 2008; Aldanmaz et al. 2009; Saccani et al. 2010; Dokuz et al. 2011; Uysal et al. 2012). Magmatic processes in the mantle wedge can contribute to this enrichment (Niu 2004). Garrido et al. (2005) suggested that serpentine dehydration is a source of LILE, Pb and Sr fluid leached from the slab and transported into the mantle wedge. However, in the case of Darreh Deh lherzolite, primary magmatic clinopyroxenes are more depleted in Sr and Ba (Fig. 4B) compared to the bulk rock (Fig. 6E), indicating that Pb, Sr and Ba could have been partially enriched after seafloor weathering and/or serpentinization (e.g. Niu 2004; Deschamps et al. 2013).

5.2.2. Clinopyroxene composition

The average Al_2O_3, Na_2O and TiO_2 concentrations and Cr# and Mg# of clinopyroxene and orthopyroxene from Darreh Deh meta-lherzolite (Fig. 8) are comparable to those from lherzolites from the central parts of this ophiolite (investigated by PIRNIA (2007)), of abyssal peridotite (e.g. CHOI et al. 2008 & references therein) and of MOR peridotites (e.g. ALDANMAZ 2012; SACCANI et al. 2010) which all have Yb>0.5 μg/g and Dy>1 μg/g (Fig. 9). In addition, the compositions of clinopyroxene and orthopyroxene in Darreh Deh harzburgite closely resemble those of SSZ peridotites (Figs. 8 and 9).

The chondrite-normalized REE patterns for clinopyroxenes in Darreh Deh lherzolite (Fig. 4A) show an affinity with the average composition of samples from PIRNIA (2007), and those of MOR mantle peridotites formed by low degrees of partial melting (e.g. Atlantis II Fracture Zone, JOHNSON & DICK 1992; Red Hills peridotite in the Dun Mountain ophiolite of South Island, New Zealand, SANO & KIMURA 2007). In contrast, the clinopyroxenes of SSZ peridotites (e.g. Hellenic Peninsula, Pindos and Bulqiza in Albania; BIZIMIS et al. 2000) are well characterized by a largely flat REE pattern with LREE enrichment. On the primitive mantle normalized diagram (Fig. 4B) the HFSE and LILE of our samples strongly overlap with those of the Red Hills MOR peridotites.

The LREE (La, Ce, Pr, Nd) and Zr abundances of clinopyroxenes from Darreh Deh lherzolites are more depleted (Fig. 4B) than the bulk-rock compositions (Fig. 6E) and in this respect they resemble clinopyroxenes of abyssal MOR peridotites (e.g. NIU 2004). The bulk rock probably underwent post-melting LREE refertilization. However, Nb shows an inverse pattern possibly caused by later serpentinization. NUI (2004) and experimental studies on distribution coefficients (FOLEY et al. 1999; GREEN et al. 2000; TIEPOLO et al. 2000) have confirmed $D_{Zr}<D_{Hf}$. Therefore, the fact that Hf/Zr of clinopyroxene (~0.22) is higher than that of bulk rock (~0.02) strongly points to control by a magmatic process rather than later serpentinization or weathering.

The correlations among Dy, Nd, Zr, Yb, and Ti in clinopyroxene (Figs. 10A, B and C) and Cr# of Cr-spinel (Fig. 10D) indicate 6 to 10% partial melting for Cretaceous lherzolites (samples from PIRNIA 2007), but slightly higher partial melting degrees for the Jurassic Darreh Deh lherzolite (this study), indicating formation by depletion of a fertile mantle peridotite by extraction of a basaltic component.

The model of WOOD & BLUNDY (1997) was used to calculate the original lherzolitic melt composition (Table 8). The melt that resulted from reaction between melt and peridotite was not only undersaturated in orthopyroxene (or silica) but also saturated in clinopyroxene (SEYLER et al. 2007). In this method, the major elements of clinopyroxene in Darreh Deh lherzolite are used to calculate the $Kd_{cpx/melt}$, Mg# and REE composition of the primitive melt in equilibrium with clinopyroxene in lherzolite. Pressure and temperature calculation were performed using the approach of NIMIS & TAYLOR (2000) and yielded an average temperature and pressure of ~1100 °C and 21 kbar. The $Kd_{cpx/melt}$ values are >1 for the HREE. Fig. 4A compares the chondrite-normalized REE patterns of clinopyroxene, calculated primitive melt and the bulk rock compositions. The HREE abundance of the calculated melt is between that of the clinopyroxene (Fig. 4A) and bulk lherzolite (Fig. 6A), indicating a MOR affinity and <10% of partial melting for the formation of Darreh Deh lherzolite.

5.2.3. Cr-spinel composition

Cr-spinel and coexisting olivine in lherzolite are within the compositional range of mid-ocean ridge peridotite (e.g. DICK 1989, PEARCE et al. 2000 & references therein). Plotting Mg# versus Cr# of Cr-spinels (Fig. 10E), it can be seen that Darren Deh lherzolite overlaps with abyssal Alpine I-type peridotites, and harzburgite with fore-arc peridotites. The low TiO_2 contents (<0.06 g/100g) of Cr-spinel from lherzolite can be attributed to their residual nature. Mn and Cr/Al increments in Cr-spinel support the partial melting model. Partial melting degrees of 7.8-8.5% and 16.8% are calculated for, respectively, Darreh Deh lherzolite and harzburgite, using the equation $F = 10x\ln(Cr\#_{spinel}) + 24$ (HELLEBRAND et al. 2001). The partial melting degrees are partly higher than calculated for samples of PIRNIA (2007). However, the higher 16.8% partial melting degree calculated for the replacive harzburgite could be related to Cr enrichment by the melt-rock reactions (and Cr release by incongruent pyroxene dissolution), rather than to partial melting (e.g. KUBO 2002).

5.3. Early Mesozoic melt-rock reaction and tectonism history in Nain Ophiolite

Early Permian to Middle Permian – Early Triassic opening of the Neo-Tethys Ocean between the Iranian and Arabian plates (e.g. AGARD et al. 2011), followed by Late Triassic closure of Paleo-Tethys ocean dur-

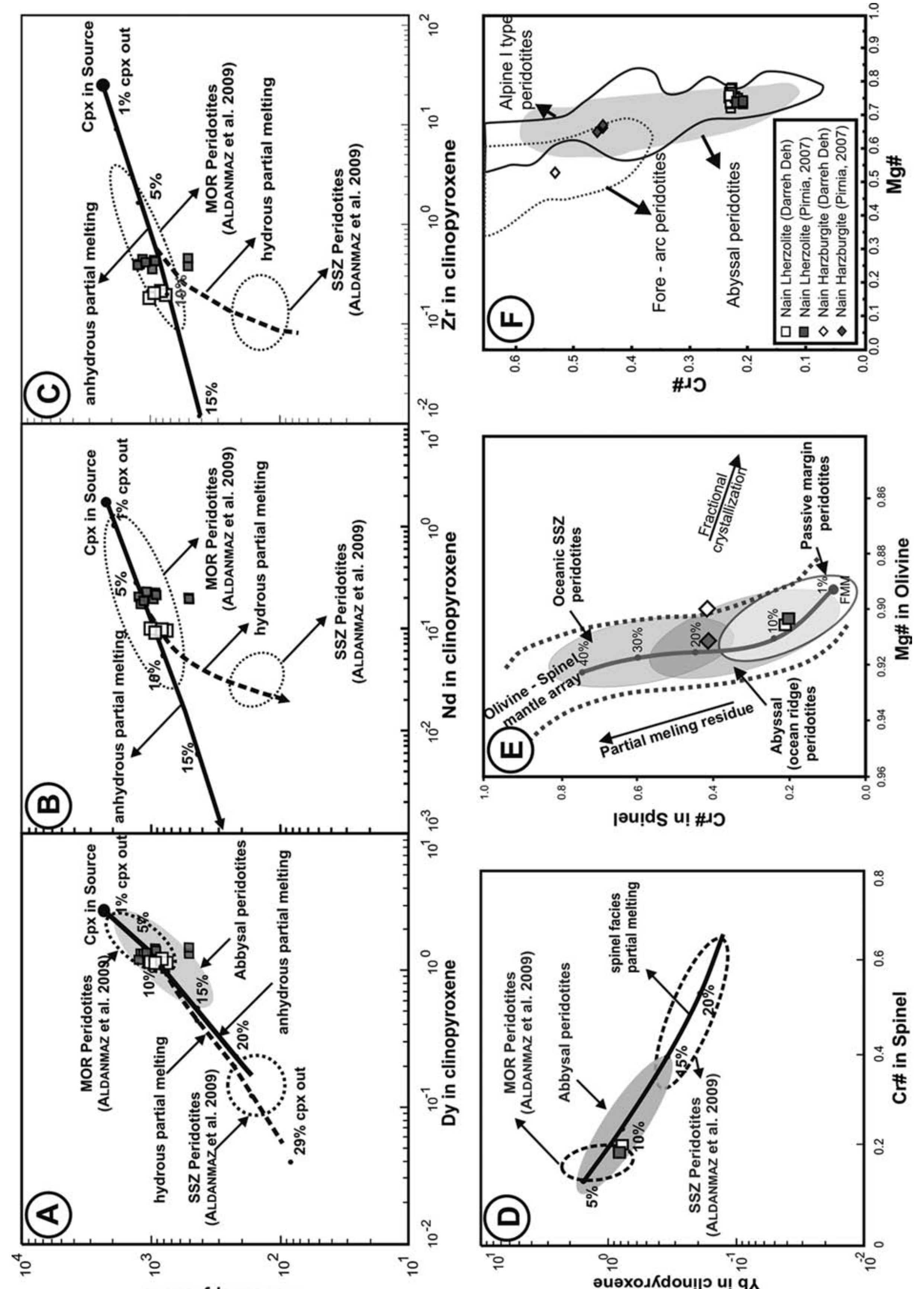
A
Ti in clinopyroxene
Dy in clinopyroxene
Cpx in Source
1% cpx out
5%
10%
15%
20%
29% cpx out
MOR Peridotites (ALDANMAZ et al. 2009)
hydrous partial melting
SSZ Peridotites (ALDANMAZ et al. 2009)
Abbysal peridotites
anhydrous partial melting
B
Nd in clinopyroxene
C
Zr in clinopyroxene
D
Yb in clinopyroxene
Cr# in Spinel
spinel facies partial melting
Abbysal peridotites
45%
E
Cr# in Spinel
Mg# in Olivine
Oceanic SSZ peridotites
Olivine - Spinel mantle array
Partial meling residue
Abyssal (ocean ridge) peridotites
Passive margin peridotites
Fractional crystallization
FMM
40%
30%
20%
1%
F
Cr#
Mg#
Alpine I type peridotites
Fore - arc peridotites
Abyssal peridotites
□ Nain Lherzolite (Darreh Deh)
■ Nain Lherzolite (Pirnia, 2007)
◇ Nain Harzburgite (Darreh Deh)
◆ Nain Harzburgite (Pirnia, 2007)

Fig. 10.

ing the Cimmerian orogeny (e.g. Samadi et al. 2014, and references therein) resulted in a complex tectonic evolution from mid-ocean ridge spreading (i.e. Triassic western branch and Jurassic eastern branch of Neo-Tethys Ocean; Fig. 11A) to intra-oceanic subduction in the Nain Ocean (Fig. 11B).

During the mid-Cimmerian Orogeny in the Early Jurassic (around 188 Ma, Table 1), partial melting of subducting Nain oceanic crust produced a tholeiitic, clinopyroxene-saturated and HREE-enriched melt that was involved in the formation of replacive harzburgite and dunite, and was emplaced as diabase dikes and lavas. The interaction between melt and lherzolitic wall rocks is characterized by formation of replacive olivine (Ol_r) due to incongruent melting of orthopyroxene, and formation of Cr-spinel in harzburgite. This produced harzburgite and eventually dunite containing secondary olivine, lower amounts of clinopyroxene, higher Cr# in Cr-spinel, flatter bulk rock chondrite-normalized HREE patterns, and extremely high bulk rock Ni/Yb ratios (>6). During these events, mantle peridotites were partially and weakly hydrated and serpentinized.

Subsequently, convergence between Sanandaj – Sirjan zone and the CEIM (Fig. 11C) caused ophiolite obduction and accretion and/or collision processes that were associated with high-grade regional metamorphism of upper amphibolite- to lower granulite-facies conditions. Metamorphism affected the complete ophiolite sequence, ranging from Darreh Deh mantle peridotites (~ 630-700 °C and 7-15 kbar) and the diabasic dikes within them, to the basalts and pillow lavas (~ 650 to 800 °C and 7-8 kbar; Shirdashtzadeh et al. 2010, 2011, Torabi et al. 2011b). Ocean floor metamorphism typically shows temperatures increasing with depth. However, the high P-T conditions of metamorphism of the Darreh Deh peridotites are similar to those calculated for the amphibolitized basic rocks (diabasic dikes within the mantle peridotites, basalts and pillow lavas; Shirdashtzadeh et al. 2010). Thus, the similar degree of metamorphism in this ophiolite sequence from its bottom (mantle peridotites and diabasic dikes) to its top (basalt and lavas) indicates that it was a consequence of accretion and/or collision processes that followed basin closure, rather than an ocean-floor metamorphism that occurred near a spreading ridge or metamorphism in an oceanic subduction zone. If, for example, metamorphism of the lherzolite had taken place in a near-ridge ocean floor setting, or during slab subduction, then we would expect different metamorphic textures in harzburgites and dunites that formed in a supra-subduction zone and at shallower depths. The melt-rock reaction would have largely overprinted and recrystallized the metamorphic textures. However, the evidence for a prograde metamorphic overprint seen in the SSZ harzburgites and dunite confirms that it occurred after the melt-rock interactions. This amphibolite-facies metamorphic stage is characterized by the formation in Darreh Deh mantle peridotites of metamorphic olivine neoblasts (Ol_2), talc and tremolite. In contrast, mantle peridotites in the central parts of the Nain Ophiolite (e.g. Pirnia 2007; Torabi 2008; Ghazi et al. 2011) lack any signs of this metamorphism as a result of serpentinization and effects of Cretaceous-age ascending melts. Cretaceous (~Albian to Cenomanian) melt–rock reactions in an SSZ system active in the Nain Ocean (Fig. 11D) produced harzburgite, dunite, gabbros, sheeted and diabasic dikes, massive basalts, and pillow lavas (e.g. Pirnia 2007; Ghazi et al. 2011; Shirdashtzadeh et al. 2011).

Finally, spreading in this ocean gradually ceased in the early Upper Cretaceous and basin closure was initiated (Fig. 11E), culminating in obduction and juxtaposition of ocean crust along the Nain – Baft fault, thus forming the Nain and Ashin ophiolites. Therefore, traces of Cretaceous-age melt-rock reactions in Nain Ophiolite are best preserved in most of the studied outcrops (e.g. Pirnia 2007; Pirnia et al. 2010; Torabi 2008; Ghazi et al. 2011), but little evidence has been found for older (Jurassic) melt-rock reactions, ex-

Fig. 10. (A), (B) and (C) Plot of Dy, Nd and Zr versus Ti of clinopyroxene in lherzolite; (D) Cr# in clinopyroxene versus Yb of spinel in lherzolite; (E) Mg# of spinel versus Cr# of olivine in lherzolite and harzburgite (Arai 1994). Diagrams modified after Aldanmaz et al. (2009). The abyssal peridotite composition is from Johnson et al. (1990), Johnson & Dick (1992) and Hellebrand et al. (2001). The SSZ peridotite composition is from Aldanmaz et al. (2009). The partial melting curves show the degree of hydrous and anhydrous partial melting. Major element oxides are in g/100g and trace elements are in μg/g), (F) Mg# versus Cr# of Cr-spinels in lherzolite and harzburgite of the Nain Ophiolite (after Arai, 1994). The abyssal and fore-arc peridotites are from Tamura & Arai (2006) and the Alpine I-type peridotites are from Dick & Bullen (1984).

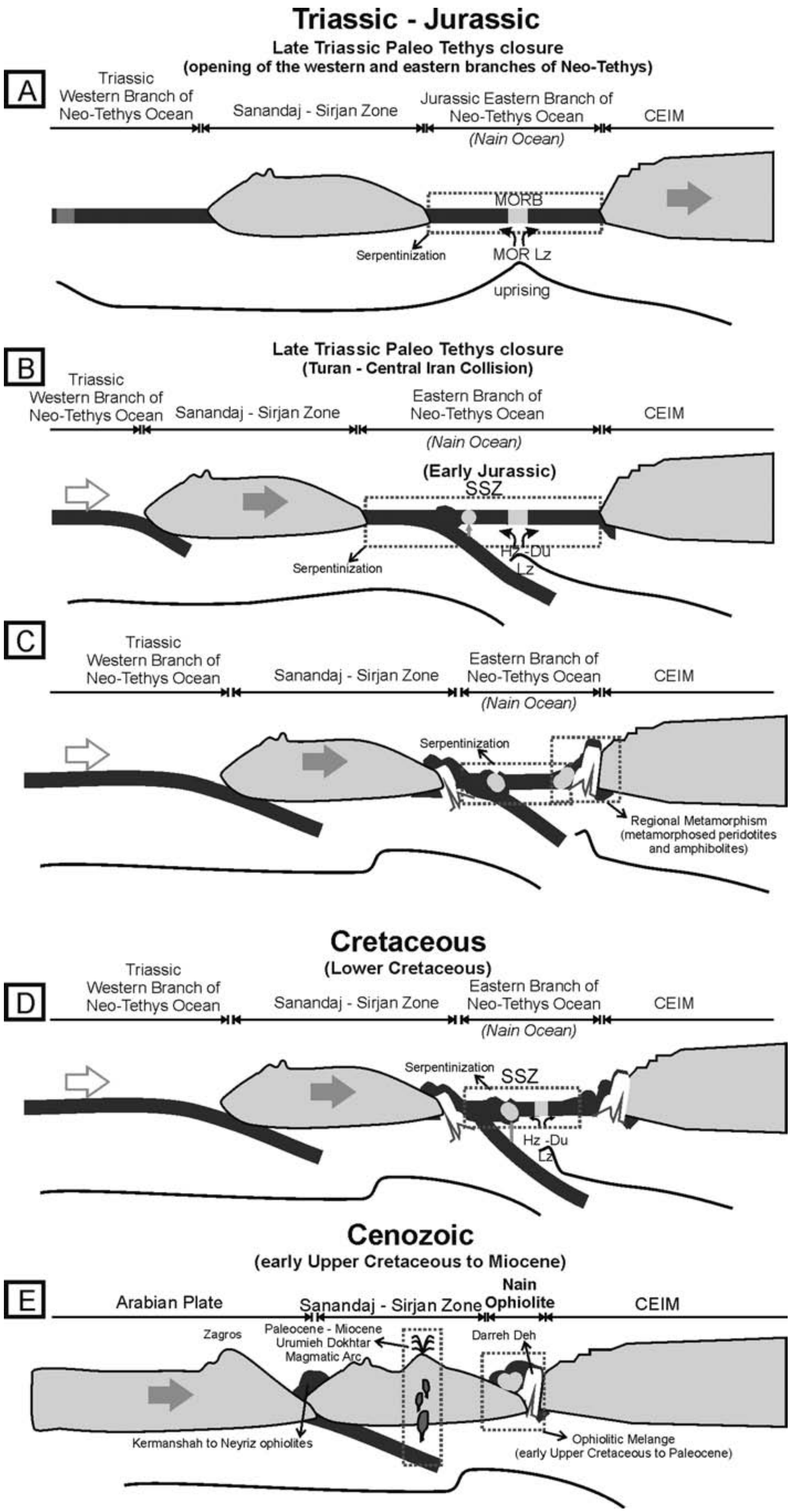
Triassic - Jurassic
Late Triassic Paleo Tethys closure
(opening of the western and eastern branches of Neo-Tethys)
A
Triassic Western Branch of Neo-Tethys Ocean
Sanandaj - Sirjan Zone
Jurassic Eastern Branch of Neo-Tethys Ocean
(Nain Ocean)
CEIM
MORB
Serpentinization
MOR Lz
uprising
Late Triassic Paleo Tethys closure
(Turan - Central Iran Collision)
B
Triassic Western Branch of Neo-Tethys Ocean
Sanandaj - Sirjan Zone
Eastern Branch of Neo-Tethys Ocean
(Nain Ocean)
CEIM
(Early Jurassic)
SSZ
Serpentinization
Hz -Du
Lz
C
Triassic Western Branch of Neo-Tethys Ocean
Sanandaj - Sirjan Zone
Eastern Branch of Neo-Tethys Ocean
(Nain Ocean)
CEIM
Serpentinization
Regional Metamorphism (metamorphosed peridotites and amphibolites)
Cretaceous
(Lower Cretaceous)
D
Triassic Western Branch of Neo-Tethys Ocean
Sanandaj - Sirjan Zone
Eastern Branch of Neo-Tethys Ocean
(Nain Ocean)
CEIM
Serpentinization
SSZ
Hz -Du
Lz
Cenozoic
(early Upper Cretaceous to Miocene)
E
Arabian Plate
Sanandaj - Sirjan Zone
Nain Ophiolite
CEIM
Zagros
Paleocene - Miocene Urumieh Dokhtar Magmatic Arc
Darreh Deh
Kermanshah to Neyriz ophiolites
Ophiolitic Melange (early Upper Cretaceous to Paleocene)

Fig. 11.

pect for the Darreh Deh peridotites (this study). Thes latter underwent amphibolite-facies metamorphism similar to the metabasic rocks in the same ophiolite (e.g. Shirdashtzadeh et al. 2010) but were preserved from serpentinization and/or overprinting by ascending melts in Cretaceous times.

6. Conclusions

The Nain Ophiolite is a remnant of the long-lived, Early Jurassic to upper Early Cretaceous - Paleocene Nain Ocean. The Jurassic Darreh Deh mantle peridotites form an individual, isolated massif exposed in the east of the Nain Ophiolite. The REE compositions of Darreh Deh metamorphosed peridotites and the clinopyroxene and Cr-spinel compositions indicate that the peridotites are comparable to published data for the Nain Ophiolite mantle peridotites, but that the Darreh Deh samples record slightly higher degrees of partial melting and more advanced melt–rock reactions. The Darreh Deh peridotites are MOR-type mantle lherzolites that later, in a supra-subduction zone setting, were transformed into harzburgite and dunite during interaction with ascending melts.

Regional metamorphism related to ophiolite obduction and accretion and/or collision processes induced by convergence between the Sanandaj – Sirjan zone and the CEIM affected the Darreh Deh ultramafic rocks. The mantle peridotites have the characteristic mineral assemblages Ol_1 + Cpx + Opx + Cr-Spl + Atg + Ol_2 + Tlc + Tr + Chl that formed under amphibolite-facies conditions of ~630-700 °C and 7-15 kbar that were similar those of metamorphosed diabasic dikes, basalts and pillow lavas in the same ophiolite.

The Nain oceanic spreading system was reactivated in the Cretaceous (~Albian to Cenomanian) and consequently, melt-rock reactions with ascending melts caused the formation of harzburgite and dunite after lherzolites. The effects of serpentinization and Cretaceous melt-rock reactions obscured the evidence for earlier, Jurassic melt-rock reactions and metamorphism in the mantle peridotites of this ophiolite, except in the Darreh Deh area in its eastern part.

Acknowledgment

The authors thank the University of Isfahan (Isfahan, Iran), Kanazawa University (Kanazawa, Japan) and Montanuniverisät (Leoben, Austria) for financial supports and providing geochemical facilities. The authors express gratitude to the constructive reviews of Dr. Samuel Angiboust and Dr. Stéphane Guillot and the editorial handling of associated editor Martin Timmerman which improved the original manuscript. Prof. Chris Harris is greatly appreciated for his constructive reviews.

References

Agard, P., Omrani, J., Jolivet, L., Whitechurch, H., Vrielynck, B., Spakman, W., Monié, P., Meyer, B. & Wortel, R. (2011): Zagros orogeny: a subduction-dominated process. – Geological Magazine, **148** (5–6): 692-725.

Aldanmaz, E. (2012): Trace element geochemistry of primary mantle minerals in spinel-peridotites from polygenetic MOR-SSZ suites of SW Turkey: constraints from an LA-ICP-MS study and implications for mantle metasomatism. – Geological Journal, **47**: 59-76.

Aldanmaz, E., Schmidt, M.W., Gourgaud, A. & Meisel, T. (2009): Mid-ocean ridge and supra-subduction geochemical signatures in spinel-peridotites from the Neotethyan ophiolites in SW Turkey: Implications for upper mantle melting processes. – Lithos, **113** (3-4): 691-708.

Angiboust, S., Agard, P., De Hoog, J.C.M., Omrani, J. & Plunder, A. (2013): Insights on deep, accretionary subduction processes from the Sistan ophiolitic “mélange” (Eastern Iran). – Lithos, **156**: 139-158.

Arai, S. (1994): Characterization of spinel peridotites by olivine-spinel compositional relationships: review and interpretation. – Chemical Geology, **113**: 191-204.

Bach, W., Garrido, C.J., Paulick, H., Harvey, J. & Rosner, M. (2004): Seawater–peridotite interactions: First insights from ODP Leg 209, MAR 15°N. – Geochemistry Geophysics Geosystems, **5 (9)**: Q09F26.

Bizimis, M., Salters, V.J.M. & Bonatti, E. (2000): Trace and REE content of clinopyroxene from suprasubduction zone peridotites. Implications for melting and enrichment processes in island arcs. – Chemical Geology, **165**: 67-85.

Bliss, M.W. & MacLean, W.H. (1975): The paragenesis of zoned chromite from central Monitaba. – Geochimica et Cosmochimica Acta, **39**: 973-990.

Bodinier, J.L., Dupuy, C. & Dostal, J. (1988): Geochemistry and petrogenesis of Eastern Pyrenean peridotites. – Geochimica et Cosmochimica Acta, **52**: 2893-2907.

Fig. 11. Tectonic evolution of the Darreh Deh area in the eastern section of the Nain Ophiolite (between the Sanandaj–Sirjan zone and the Central-East Iranian Microplate) (modified after Shirdashtzadeh et al. 2011).

Bröcker, M., Fotoohi Rad, G., Burgess, R., Theunissen, S., Paderin, I., Rodionov, N. & Salimi, Z. (2013): New age constraints for the geodynamic evolution of the Sistan Suture Zone, eastern Iran. – Lithos, **170-171**: 17-34.

Bucher, K. & Grapes, R. (2011): Petrogenesis of Metamorphic Rocks. – 428 pp.; Springer-Verlag, Berlin.

Choi, S.H., Shervais, J.W. & Mukasa, S.B. (2008): Suprasubduction and abyssal mantle peridotites of the Coast Range ophiolite, California. – Contributions to Mineralogy and Petrology, **156**: 551-576.

Coleman, R.G. (1977): Ophiolites: Ancient oceanic lithosphere. – 229 pp.; Springer-Verlag, Berlin.

Collier, M.L. & Keleman, P.B. (2010): The Case for Reactive Crystallization at Mid-Ocean Ridge. – Journal of Petrology, **51**: 1913-1940.

Connolly, J.A.D. (1990): Multivariable phase diagrams: an algorithm based on generalized thermodynamics. – American Journal of Science, **290**: 666-718.

Davoudzadeh, M. (1972): Geology and petrography of the area north of Nain, Central Iran. – 89 pp.; Geological Survey of Iran, Report No. 39.

Debret, B., Andreani, M., Godard, M., Nicollet, C., Schwartz, S. & Lafay, R. (2013): Trace element behavior during serpentinization/de-serpentinization of an eclogitized oceanic lithosphere: A LA-ICPMS study of the Lanzo ultramafic massif (Western Alps). – Chemical Geology, **357**: 117-133.

Deschamps, F., Godard, M., Guillot, S. & Hattori, K. (2013): Geochemistry of subduction zone serpentinites: A review. – Lithos, **178**: 96-127.

Dick, H.J.B. & Bullen, T. (1984): Chromian spinel as a petrogenetic indicator in abyssal and alpine-type peridotites and spatially associated lavas. – Contributions to Mineralogy and Petrology, **86**: 54-76.

Dick, H.J.B. (1989): Abyssal peridotites, very slow spreading ridges and ocean ridge magmatism. – In: Saunders, A.E. & Norris, M.J. (Eds): Magmatism in the ocean basins, **42**: 71-105; Geological Society, Specific Publication.

Dilek, Y. & Newcomb, S. (2003): Ophiolite concept and the evolution of geological thought. – 504 pp.; Geological Society of America, Special Paper 373.

Dokuz, A., Uysal, İ., Kaliwoda, M., Karsli, O., Ottley, C.J. & Kandemir, R. (2011): Early abyssal- and late SSZ-type vestiges of the Rheic oceanic mantle in the Variscan basement of the Sakarya Zone, NE Turkey: Implications for the sense of subduction and opening of the Paleotethys. – Lithos, **127 (1-2)**: 176-191.

Droop, G.T.R. (1987): A general equation for estimating Fe^{3+} concentrations in ferromagnesian silicates and oxides from microprobe analyses, using stoichiometric criteria. – Mineralogical Magazine, **51**: 431-435.

Dungan, M.A. (1979): A microprobe study of antigorite and some serpentine pseudomorphs. – Canadian Mineralogist, **17**: 771-784.

Evans, B.W. (2004): The serpentinite multisystem revisited: chrysotile is metastable. – International Geology Review, **46**: 479-506.

Evans, B.W. (1977): Metamorphism of Alpine peridotite and serpentinite. – Annual Review of Earth and Planetary Sciences, **7**: 397-447.

Evans, B.W., Johannes, W., Oterdoom, H. & Trommsdorff, V. (1976): Stability of chrysotile and antigorite in the serpentinite multi-system. – Schweizer Mineralogische und Petrographische Mitteilungen, **56**: 79-93.

Foley, S.F., Matthias, G.B. & Jenner, G.A. (1999): Rutile/melt partition coefficients for trace elements and an assessment of the influence of rutile on the trace element characteristics of subduction zone magmas. – Geochimica et Cosmochimica Acta, **64**: 933-938.

Garrido, C.J., López Sànchez-Vizcaíno, V., Gómez-Pugnaire, M.T., Trommsdorff, V., Alard, O., Bodinier, J.L. & Godard, M. (2005): Enrichment of HFSE in chlorite- harzburgite produced by high-pressure dehydration of antigorite-serpentinite: implications for subduction magmatism. – Geochemistry Geophysics Geosystems, **6**: Q01J15.

Ghasemi, A. & Talbot, C.J. (2006): A new tectonic scenario for the Sanandaj – Sirjan Zone (Iran). – Journal of Asian Earth Sciences, **26**: 683-693.

Ghazi, J.M., Moazzen, M., Rahgoshay, M. & Moghadam, H.S. (2011): The geodynamic setting of the Nain ophiolites, central Iran: evidence from chromian spinels in the chromitites and associated rocks. – Ofioliti, **36** (1): 59-76.

Glennie, K.W. (1992): Plate Tectonics & the Oman Mountains. – Tribulus, **2** (2): 11-21.

Godard, M., Lagabrielle, Y., Alard, O. & Harvey, J. (2008): Geochemistry of the highly de- pleted peridotites drilled at ODP Sites 1272 and 1274 (Fifteen-Twenty Fracture Zone, Mid-Atlantic Ridge): implications for mantle dynamics beneath a slow spreading ridge. – Earth and Planetary Science Letters, **267**: 410-425.

Green, T.H., Blundy, J.D., Adam, J.R.K. & Yaxley, G.M. (2000): SIMS determination of trace element partition coefficients between garnet, clinopyroxene and hydrous basaltic liquids at 2-7·5GPa and 1080-1200 °C. – Lithos, **53**: 165-187.

Guillot, S., Hattori, K., Agard, P., Schwartz, S., Vidal, O., Lallemand, S. & Funiciello, F. (2009): Exhumation Processes in Oceanic and Continental Subduction Contexts: A Review, Subduction Zone Geodynamics. – Frontiers in Earth Sciences, 175-205.

Hassanipak, A.A. & Ghazi, A.M. (2000): Petrochemistry, ^{40}Ar-^{39}Ar ages and tectonics of the Nain Ophiolite. Central Iran. – GSA Annual meeting, Reno, Nevada 237-238.

Hayakawa, T., Kubo, T., Kato, T. & Kikegawa, T. (2006): Dehydration sequence of chrysotile serpentine at high pressure. – 23(B): 184 pp.; Photon Factory Activity Report 2005.

Hellebrand, E., Snow, J.E. & Hofmann, A.W. (2001): Coupled major and trace elements as indicators of the extent of melting in midocean-ridge peridotites. – Nature, **410** (6829): 677-681.

Hey, M.H. (1954): A new review of the chlorites. – Mineralogical Magazine, **30**: 277-292.

Holland, T.J.B. & Powell, R. (1998): An internally consistent thermodynamic data set for phases of petrological interest. – Journal of Metamorphic Geology, **16**: 309-343.

Hoog, J.C.M., De, Gall, L. & Cornell, D.H. (2010): Trace-element geochemistry of mantle olivine and application to mantle petrogenesis and geothermobarometry. – Chemical Geology, **270** (1-4): 196-215.

Johnson, K.T.M. & Dick, H.J.B. (1992): Open system melting and temporal and spatial variation of peridotite and basalt at the Atlantis II Fracture Zone. – Journal of Geophysical Research, **97**: 9219-9241.

Johnson, K.T.M., Dick, H.J.B. & Shimizu, N. (1990): Melting in the oceanic upper mantle: An ion microprobe study of diopsides in abyssal peridotites. - Journal of Geophysical Research: Solid Earth, **95** (B3): 2661-2678.

Khedr, M.Z. & Arai, S. (2012): Petrology and geochemistry of prograde deserpentinized peridotites from Happo-One, Japan: Evidence of element mobility during deserpentinization. – Journal of Asian Earth Sciences, **43** (1): 150-163.

Kubo, K. (2002): Dunite formation processes in highly depleted peridotite: case study of the Lwanaidake peridotite, Hokkaido, Japan. – Journal of Petrology, **43**: 423-448.

Lafay, R., Deschamps, F., Schwartz, S., Guillot, S., Godard, M., Debret, B. & Nicollet, C. (2013): High-pressure serpentinites, a trap-and-release system controlled by metamorphic conditions: Example from the Piedmont zone of the western Alps. – Chemical Geology, **343**: 38-54.

Leake, B.E., Woolley, A.R., Arps, C.E.S., Birch, W.D., Gilbert, M.C., Grice, J.D., Hawthorne, F.C., Kato, A., Kisch, H.J., Krivovichev, V.G., Linthout, K., Laird, J., Mandarino, J.A., Maresh, V.W., Nickel, E.H., Rock, N.M.S., Schumacher, J.C., Smith, D.C., Stephenson, N.N., Ungaretti, L., Whittaker, E.J.W. & Youzhi, G. (1997): Nomenclature of amphiboles: report of the subcommittee on amphiboles of the International Mineralogical Association, Commission on New Minerals and Mineral Names. – American Mineralogist, **82**: 1019-1037.

McDonough, W.F. & Sun, S.S. (1995): The composition of the Earth. – Chemical Geology, **120**: 223-253.

Meisel, T., Schöner, N., Paliulionyte, V. & Kahr, E. (2002): Determination of Rare Earth Elements (REE), Y, Th, Zr, Hf, Nb and Ta in geological reference materials G-2, G-3, SCo-1 and WGB-1 by sodium peroxide sintering and ICP-MS. – Geostandards Newsletter, **26** (1): 53-61.

Moghadam, H.S., Fernando, C. & Stern, R.J. (2013): U-Pb zircon ages of Late Cretaceous Nain-Dehshir ophiolites, Central Iran. – Journal of the Geological Society, **170**: 175-184.

Moghadam, H.S., Whitechurch, H., Rahgoshay, M. & Monsef, I. (2009): Significance of Nain-Baft ophiolitic belt (Iran): Short-lived, transtensional Cretaceous back-arc oceanic basins over the Tethyan subduction zone. – Comptes Rendus Geoscience, **341**: 1016-1028.

Müntener, O., Hermann, J. & Trommsdorff, V. (2000): Cooling History and Exhumation of Lower-Crustal Granulite and Upper Mantle (Malenco, Eastern Central Alps). – Journal of Petrology, **41** (2): 175-200.

Muttoni, G., Gaetani, M., Kent, D.V., Sciunnach, D., Angiolini, L., Berra, F., Garzanti, E., Mattei, M. & Zanchi, A. (2009): Opening of the Neo-Tethys Ocean and the Pangea B to Pangea A transformation during the Permian. – GeoArabia, **14** (4): 17-48.

Nadimi, A. & Sohrabi, A. (2008): Nain tectonic mélanges, Central Iran: Strike slip faulting and tectonic evolutions. – Bollettino di Geofisica, **49** (2): 84-88.

Nicolas, A. (1989): Structures of ophiolites and dynamics of oceanic lithosphere. – 367 pp.; Dordrecht (Kluwer Academic Publishers).

Nimis, P. & Taylor, W.R. (2000): Single clinopyroxene thermobarometry for garnet peridotites. Part I. Calibration and testing of a Cr-in-Cpx barometer and an enstatite-in-Cpx thermometer. – Contributions to Mineralogy and Petrology, **71**: 13-22.

Niu, Y. (2004): Bulk-rock major and trace element compositions of abyssal peridotites: Implications for mantle melting, melt extraction and post-melting processes beneath mid- ocean ridge. – Journal of Petrology, **45**: 2423-2458.

Nozaka, T. (2014): Metasomatic hydration of the Oeyama forearc peridotites: Tectonic implications. – Lithos, **184-187**: 346-360.

Parkinson, I.J. & Pearce, J.A. (1998): Peridotites from the Izu-Bonin-Mariana Forearc (ODP Leg 125): Evidence for Mantle Melting and Melt-Mantle Interaction in a Supra-Subduction Zone Setting. – Journal of Petrology, **39** (9): 1577-1618.

Paulick, H., Bach, W., Godard, M., De Hoog, J.C.M., Suhr, G. & Harvey, J. (2006): Geochemistry of abyssal peridotites (Mid- Atlantic Ridge, 15°20'N, ODP Leg 209): Implications for fluid/rock interaction in slow spreading environments. – Chemical Geology, **234**: 179-210.

Pearce, J.A., Barker, P.F., Edwards, S.J., Parkinson, I.J. & Leat, P.T. (2000): Geochemistry and tectonic significance of peridotites from the South Sandwich arc-basin system, south Atlantic. – Contributions to Mineralogy and Petrology, **139**: 36-53

Pearce, J.G., Perkins, W.T., Westgate, J.A., Gorton, M.P., Jackson, S.E., Neal, C.R. & Chenery, S.P. (1997): A compilation of new and published major and trace element data for NIST SRM 610 and NIST SRM 612 glass reference materials. – Geostandards Newsletter: The Journal of Geostandards and Geoanalysis, **21**: 114-144.

Pirnia, T. (2007): Petrology of Nain Ophiolite mantle peridotites (Isfahan province). – 193 pp.; M.Sc. Thesis in Petrology, Department of Science, Isfahan University, Iran.

Pirnia, T., Arai, S. & Torabi, G. (2010): Post-deformational impregnation of depleted MORB in Nain lherzolite (Central Iran). – Journal of Mineralogical and Petrological Sciences, **105**: 74-79.

Reichert, J. (2007): A metallogenetic model for carbonate-hosted non-sulphide zinc deposits based on observations of Mehdi Abad and Irankuh, Central and Southwestern Iran. – 157 pp.; Ph.D. Thesis, Martin Luther University, Halle Wittenberg.

Rietmeijer, F.J.M. (1983): Chemical distinction between igneous and metamorphic orthopyroxenes especially those coexisting with Ca-rich clinopyroxenes: a re-evaluation. – Mineralogical Magazine, **47**: 143-151.

Saccani, E., Delavari, M., Beccaluva, L. & Amini, S. (2010): Petrological and geochemical constraints on the origin of the Nehbandan ophiolitic complex (eastern Iran): Implication for the evolution of the Sistan Ocean. – Lithos, **117** (1-4): 209-228.

Samadi, R., Gazel, E., Mirnejad, H., Kawabata, H., Baharifar, A.A. & Sheikh Zakariaee, S.J. (2014): Triassic Paleo-Tethys subduction in the center of the Alpine-Himalayan Orogen: Evidence from Dehnow I-type granitoids (NE Iran). – Neues Jahrbuch für Geologie und Palaontologie, **271** (3): 285-306.

Sano, S. & Kimura, J.I. (2007): Clinopyroxene REE geochemistry of the Red Hills Peridotite, New Zealand: interpretation of magmatic processes in the upper mantle and in the Moho transition zone. – Journal of Petrology, **48**: 113-139.

Schwartz, S., Guillot, S., Reynard, B., Lafay, R., Debret, B., Nicollet, C., Lanari, P., Auzende, A.L. (2013): Pressure-temperature estimates of the lizardite/antigorite transition in high pressure serpentinites. – Lithos, **178** (15): 197-210.

Seyler, M., Lorand, J.P., Dick, H.J.B. & Drouin, M. (2007): Pervasive melt percolation reactions in ultra-depleted refractory harzburgites at the Mid-Atlantic Ridge, 15°20' N: ODP Hole 1274A. – Contributions to Mineralogy and Petrology, **153** (3): 303-319.

Sharkovski, M., Susov, M. & Krivyakin, B. (1984): Geology of the Anarak area (Central Iran), – 143 pp.; V/O Technoexport Report TE/No. 19, Moscow.

Shervais, J.W., Kolesar, P. & Andreasen, K. (2005): Field and Chemical Study of Serpentinization-Stonyford, California: Chemical Fluxes and Mass Balance. – International Geology Review, **47**: 1-23.

Shirdashtzadeh, N. (2007): Petrology of metamorphic rocks of Nain ophiolitic mélange (Isfahan province). – 192 pp.; M. Sc. Thesis in Petrology, Department of Science, Isfahan University, Iran.

Shirdashtzadeh, N. (2014): Petrology of pillow lavas and amphibolites and metamorphism in mantle peridotites of Nain and Ashin ophiolites. – 345 pp.; Ph.D. Thesis in Petrology, Department of Science, Isfahan University, Iran.

Shirdashtzadeh, N., Torabi, G. & Arai, S. (2010): Metamorphism and metasomatism in the Jurassic of Nain ophiolitic mélange, Central Iran. – Neues Jahrbuch für Geologie und Paläontologie, Abhandlungen, **255** (3): 255-275.

Shirdashtzadeh, N., Torabi, G. & Arai, S. (2011): Two Mesozoic oceanic phases recorded in the basic and metabasic rocks of the Nain and Ashin-Zavar ophiolitic mélanges (Isfahan Province, Central Iran). – Ofioliti, **36** (2): 191-205.

Snow, J.E. & Dick, H.J.B. (1995): Pervasive magnesium loss by marine weathering of peridotite. – Geochimica et Cosmochimica Acta, **59**: 4219-4235.

Spear, F.S. (1995): Metamorphic Phase Equilibria and Pressure-Temperature-Time Paths. – 799 pp.; Monograph, Mineralogical Society of America, Washington, 970 H.

Tamura, A. & Arai, S. (2006): Harzburgite-dunite-orthopyroxenite suite as a record of supra-subduction zone setting for the Oman ophiolite mantle. – Lithos, **90**: 43-56.

Taylor, S.R. & McLennan, S.M. (1985): The continental crust: Its composition and evolution. – 312 pp.; Oxford (Blackwell).

Tiepolo, M., Vannucci, R., Oberti, R., Foley, S., Bottazzi, P. & Zanetti, A. (2000): Nb and Ta incorporation and fractionation in titanian pargasite and kaersutite: crystal-chemical constraints and implications for natural systems. – Earth and Planetary Science Letters, **176**: 185-201.

Torabi, G., Arai, S. & Koepke, J. (2011a): Metamorphosed mantle peridotites from Central Iran (Jandaq area, Isfahan province). – Neues Jahrbuch für Geologie und Paläontologie, Abhandlungen, **261**: 129-150.

Torabi, G. (2004): Petrology of ophiolites in Anarak area, northeast of Isfahan province, Iran. – 240 pp.; Ph.D. Thesis in petrology, Tarbiat Modares University, Iran.

Torabi, G. (2008): Ultramafic hornfels in Central Iran ophiolites. – Journal of Applied Sciences, **8**: 2031-2040.

Torabi, G. (2010): Early Oligocene alkaline lamprophyric dykes from the Jandaq area (Isfahan Province, Central Iran): Evidence of Central-East Iranian microcontinent confining oceanic crust subduction. – Island Arc, **19**: 277-291.

Torabi, G. (2013): Chromitite absence, presence and chemical variation in ophiolites of Central Iran (Naein, Ashin, Anarak and Jandaq). – Neues Jahrbuch für Geologie und Paläontologie, Abhandlungen, **267** (2): 171-192.

Torabi, G., Shirdashtzadeh, N., Arai, S. & Koepke, J. (2011b): Paleozoic and Mesozoic ophiolites of Central Iran: amphibolites from Jandaq, Posht-e-Badam, Nain and Ashin ophiolites. – Neues Jahrbuch für Geologie und Paläontologie, Abhandlungen, **262** (2): 227-240.

Uysal, I., Ersoy, E.Y., Karsli, O., Dilek, Y., Sadiklar, M.B., Ottley, C.J., Tiepolo, M. & Meisel, T. (2012): Coexistence of abyssal and ultra-depleted SSZ type mantle peridotites in a Neo-Tethyan Ophiolite in SW Turkey: Constraints from mineral composition, whole-rock geochemistry (major-trace-REE-PGE), and Re-Os isotope systematics. – Lithos, **132-133**: 50-69.

Whitney, D.L. & Evans, B.W. (2010): Abbreviations for names of rock-forming minerals. – American Mineralogist, **95**: 185-187.

Wicks, F.J. & Plant, A.G. (1979): Electron microprobe and X-ray micro beam studies of serpentine textures. – Canadian Mineralogist, **17**: 785-830.

Wood, B.J. & Blundy, J.D. (1997): A predictive model for rare earth element partitioning between clinopyroxene and anhydrous silicate melt. – Contributions to Mineralogy and Petrology, **129**: 166-181.

Worden, R.H., Droop, G.T.R. &Champness, P.E. (1991): The reaction antigorite → olivine + talc + H_2O in the Bergell aureole, N. Italy. – Mineralogical Magazine, **55**: 367-377.

Xu, Y.G., Martin, A., Menzies, M., Thirlwall, F., Huang, X.L., Liu, Y. & Chen, X.M. (2003): "Reactive" harzburgites from Huinan, NE China: Products of the lithosphere asthenosphere interaction during lithospheric thinning? – Geochimica et Cosmochimica Acta, **67** (3): 487-505.

Manuscript received: December 7th, 2013.
Revised version accepted by the Potsdam editor: June 2nd, 2014.

Addresses of the authors:

Nargess Shirdashtzadeh (corresponding author), Department of Geology, Faculty of Science, University of Isfahan, Isfahan, Iran;
e-mail: nshirdasht@sci.ui.ac.ir

Ghodrat Torabi, Department of Geology, Faculty of Science, University of Isfahan, Isfahan, Iran.
Thomas Meisel, General and Analytical Chemistry, Montanuniversität, 8700 Leoben, Austria.

Shoji Arai, Department of Earth Sciences, Kanazawa University, Kanazawa, Japan.
Syed Nadeem Hussain Bokhari, General and Analytical Chemistry, Montanuniversität, 8700 Leoben, Austria.
Ramin Samadi, Department of Geology, College of Basic Sciences, Tehran Science and Research Branch, Islamic Azad University, Tehran, Iran.

Esteban Gazel, Department of Geosciences, Virginia Tech, 4044 Derring Hall (0420), Blacksburg, VA 24061, USA.

Table 1. Published K/Ar, Ar/Ar and U-Pb age results for gabbros, plagiogranite and tonalitic dikes in the Nain Ophiolite.

Reference	Method	Mineral	Rock type	Age (Ma)
Moghadam et al. (2013)	U-Pb	Zircon	Plagiogranite	102.6-103.1
Moghadam et al. (2009)	K-Ar	Amphibole	Amphibole-bearing gabbros	93.4±3.6
Hassanipak & Ghazi (2000)	Ar-Ar	Amphibole	Hornblende gabbro	101.2±0.9
				99.7±0.9
				99±1.2
Sharkovski et al. (1984)	K-Ar	Amphibole	Gabbro-plagiogranite[1]	188
			Gabbro-plagiogranite[2]	98

Table 2. Representative microprobe data for olivines from metamorphosed Darreh Deh peridotites, and their calculated structural formula based on 4 oxygen atoms (Hz = harzburgite, Lhz = lherzolite, Ol_1 = magmatic olivine, Ol_2 = metamorphic olivine, Ol_r = replacive olivine). Note: bd = below detection limit.

Rock type	Lhz																	Hz					
Olivine type	Ol_1	Ol_1	Ol_1	Ol_1	Ol_1	Ol_1	Ol_1	Ol_2	Ol_2	Ol_2	Ol_2	Ol_2	Ol_2	Ol_2	Ol_2	Ol_2	Ol_2	Ol_r	Ol_r	Ol_r	Ol_r	Ol_r	Ol_r
Point no.	23	24	25	32	33	34	35	26	27	30	31	39	40	41	42	43	45	99	100	104	106	108	329
(g/100g)																							
SiO_2	40.92	40.68	40.80	40.71	40.75	40.44	40.78	40.85	40.84	40.15	40.49	40.69	40.24	40.42	40.76	40.79	40.33	40.47	40.66	40.53	40.52	40.37	40.85
TiO_2	bd	bd	0.02	bd	0.01	bd	0.01	bd	bd	bd	bd	bd	bd	bd	bd	bd	bd	bd	bd	bd	bd	0.01	bd
Al_2O_3	bd	bd	bd	bd	0.01	bd	bd	bd	bd	bd	bd	bd	bd	bd	bd	bd	bd	bd	bd	0.01	bd	bd	bd
Cr_2O_3	bd	bd	bd	bd	bd	bd	bd	bd	bd	bd	bd	bd	bd	bd	bd	bd	bd	bd	bd	bd	bd	bd	bd
FeO	9.50	9.42	9.56	9.57	9.75	9.57	9.48	9.47	10.03	9.71	10.12	9.67	9.61	9.66	9.69	9.41	9.61	10.29	10.53	10.25	10.64	10.54	10.08
MnO	0.13	0.14	0.10	0.14	0.17	0.13	0.17	0.13	0.12	0.14	0.11	0.11	0.17	0.10	0.15	0.13	0.11	0.15	0.15	0.14	0.13	0.16	0.12
MgO	49.98	49.87	49.81	49.87	50.07	50.06	50.11	49.82	49.65	49.76	49.75	49.84	49.31	50.28	49.97	49.97	49.67	49.49	49.39	49.74	49.42	49.50	48.42
CaO	0.03	0.03	0.04	0.04	0.03	0.02	0.03	0.02	bd	bd	bd	bd	bd	0.01	0.00	0.01	0.01	0.03	0.04	bd	0.02	0.03	0.02
Na_2O	bd	bd	bd	bd	bd	bd	bd	bd	bd	bd	bd	0.01	bd	bd	bd	bd	bd	bd	bd	bd	bd	0.01	0.00
K_2O	bd	bd	bd	bd	bd	bd	bd	bd	bd	bd	bd	bd	bd	bd	bd	bd	bd	bd	bd	bd	bd	bd	bd
NiO	0.36	0.37	0.36	0.38	0.37	0.35	0.38	0.37	0.37	0.36	0.34	0.36	0.34	0.35	0.35	0.33	0.37	0.39	0.40	0.36	0.39	0.35	0.39
Sum	100.93	100.50	100.69	100.71	101.17	100.56	100.99	100.64	101.00	100.13	100.81	100.68	99.67	100.82	100.92	100.65	100.10	100.81	101.16	101.03	101.11	100.97	99.88
(a.p.f.u.)																							
Si	0.99	0.99	0.99	0.99	0.99	0.99	0.99	0.99	0.99	0.99	0.99	0.99	0.99	0.98	0.99	0.99	0.99	0.99	0.99	0.99	0.99	0.99	1.00
Ti	-	-	-	-	-	-	-	-	-	-	-	-	-	-	-	-	-	-	-	-	-	-	-
Al	-	-	-	-	-	-	-	-	-	-	-	-	-	-	-	-	-	-	-	-	-	-	-
Cr	-	-	-	-	-	-	-	-	-	-	-	-	-	-	-	-	-	-	-	-	-	-	-
Fe^{2+}	0.19	0.19	0.20	0.20	0.20	0.20	0.19	0.19	0.20	0.20	0.21	0.20	0.20	0.20	0.20	0.19	0.20	0.21	0.22	0.21	0.22	0.22	0.21
Mn	-	-	-	-	-	-	-	-	-	-	-	-	-	-	-	-	-	-	-	-	-	-	-
Mg	1.81	1.81	1.81	1.81	1.81	1.82	1.81	1.81	1.80	1.82	1.81	1.81	1.81	1.83	1.81	1.81	1.82	1.80	1.79	1.81	1.80	1.80	1.77
Ca	-	-	-	-	-	-	-	-	-	-	-	-	-	-	-	-	-	-	-	-	-	-	-
Na	-	-	-	-	-	-	-	-	-	-	-	-	-	-	-	-	-	-	-	-	-	-	-
K	-	-	-	-	-	-	-	-	-	-	-	-	-	-	-	-	-	-	-	-	-	-	-
Ni	0.01	0.01	0.01	0.01	0.01	0.01	0.01	0.01	0.01	0.01	0.00	0.01	0.00	0.01	0.01	0.00	0.01	0.01	0.01	0.01	0.01	0.01	0.01
Sum	3.00	3.01	3.00	3.01	3.01	3.01	3.01	3.00	3.00	3.01	3.01	3.01	3.01	3.01	3.01	3.01	3.01	3.01	3.01	3.01	3.01	3.01	2.99
Forsterite	90.36	90.42	90.28	90.28	90.15	90.32	90.40	90.37	89.82	90.13	89.75	90.19	90.14	90.28	90.19	90.44	90.21	89.56	89.32	89.64	89.23	89.33	89.54
Fayalite	9.64	9.58	9.72	9.72	9.85	9.68	9.60	9.64	10.18	9.87	10.25	9.81	9.86	9.73	9.81	9.56	9.79	10.44	10.68	10.36	10.77	10.67	10.46

Table 3. Representative microprobe data for clinopyroxene and orthopyroxene in Darreh Deh metamorphosed peridotites and calculated structural formula based on 6 oxygen atoms (Hz = harzburgite, Lhz = lherzolite). LA-ICP-MS data of samples marked with "*" are listed in Table 4.

Rock type	Lhz																				Hz				
Mineral type	CPX													OPX							CPX			OPX	
Point no.	904	903	902	901	37	67	294	77	76	66	314	85	93	302	72	73	296	316	94	88	86	107	102	103	101	105
(g/100g)																										
SiO_2	51.76	51.62	51.84	51.94	51.14	51.09	51.36	50.77	51.20	51.13	51.14	51.17	52.11	54.41	54.57	54.55	54.41	52.90	54.42	54.27	54.34	52.30	52.07	52.06	55.78	55.42
TiO_2	0.16	0.14	0.17	0.13	0.14	0.14	0.15	0.16	0.15	0.16	0.15	0.15	0.12	0.05	0.07	0.05	0.05	0.07	0.06	0.06	0.07	0.19	0.21	0.21	0.08	0.06
Al_2O_3	6.04	5.76	5.88	5.80	5.94	5.91	5.98	5.79	5.66	6.04	6.11	6.30	6.19	4.77	4.78	4.54	4.77	4.95	4.85	4.56	4.79	4.17	3.28	3.48	2.52	2.54
Cr_2O_3	1.10	1.07	1.14	1.10	1.20	1.08	1.06	1.16	1.13	1.10	1.16	1.19	1.13	0.68	0.69	0.71	0.68	0.84	0.75	0.77	0.75	1.10	1.10	1.14	0.70	0.71
FeO	3.41	2.90	2.86	2.99	3.21	3.18	3.21	2.95	3.18	3.41	3.27	3.38	4.53	5.91	5.95	6.14	5.91	5.46	6.27	5.90	6.28	3.90	2.95	2.91	6.78	6.51
MnO	0.08	0.08	0.09	0.10	0.12	0.09	0.12	0.11	0.10	0.08	0.08	0.10	0.12	0.13	0.14	0.13	0.13	0.12	0.12	0.13	0.13	0.11	0.10	0.09	0.16	0.15
MgO	18.57	16.62	16.78	16.63	16.90	17.12	17.06	17.41	17.51	18.21	17.57	17.21	20.71	31.53	32.17	32.39	31.53	29.40	31.95	30.95	32.00	20.13	17.26	16.45	32.96	32.44
CaO	19.56	22.20	22.13	21.90	21.15	21.27	20.79	20.95	20.64	19.56	21.42	20.09	15.66	1.79	1.64	1.57	1.79	3.89	1.99	3.39	1.66	18.12	22.31	23.06	1.58	2.26
Na_2O	0.22	0.26	0.26	0.29	0.29	0.24	0.23	0.28	0.31	0.22	0.19	0.21	0.17	0.02	0.01	0.00	0.02	0.04	0.03	0.03	0.02	0.22	0.24	0.22	0.01	0.03
K_2O	bd	bd	bd	0.01	bd	0.01	bd	bd	bd	bd	bd	bd	bd	0.01	0.01	0.00	0.01	0.00	0.00	0.00	0.00	bd	bd	bd	0.01	bd
NiO	0.06	0.07	0.04	0.06	0.04	0.04	0.03	0.04	0.06	0.06	0.04	0.06	0.08	0.09	0.08	0.07	0.09	0.08	0.11	0.07	0.11	0.07	0.04	0.06	0.07	0.09
Sum	100.96	100.71	101.18	100.92	100.13	100.17	100.00	99.62	99.94	99.97	101.13	99.87	100.81	99.39	100.12	100.17	99.39	97.75	100.53	100.11	100.15	100.32	99.56	99.67	100.63	100.20
(a.p.f.u.)																										
Si	1.85	1.86	1.86	1.87	1.85	1.85	1.86	1.84	1.85	1.85	1.83	1.86	1.86	1.90	1.89	1.89	1.90	1.89	1.88	1.88	1.88	1.88	1.90	1.90	1.92	1.92
Ti	-	-	0.01	-	-	-	-	-	-	-	-	-	-	-	-	-	-	-	-	-	-	0.01	0.01	0.01	-	-
Al^{IV}	0.15	0.14	0.14	0.13	0.15	0.15	0.14	0.16	0.15	0.15	0.17	0.14	0.14	0.10	0.11	0.12	0.10	0.12	0.12	0.12	0.12	0.12	0.10	0.10	0.08	0.08
Al^{VI}	0.11	0.11	0.11	0.12	0.11	0.10	0.12	0.09	0.10	0.10	0.09	0.13	0.12	0.09	0.08	0.07	0.09	0.09	0.07	0.07	0.08	0.05	0.04	0.05	0.02	0.02
Cr	0.03	0.03	0.03	0.03	0.03	0.03	0.03	0.03	0.03	0.03	0.03	0.03	0.03	0.02	0.02	0.02	0.02	0.02	0.02	0.02	0.02	0.03	0.03	0.03	0.02	0.02
Fe^{3+}	0.02	0.01	0.01	-	0.02	0.03	-	0.04	0.03	0.02	0.05	-	0.00	-	0.01	0.02	-	-	0.03	0.02	0.02	0.04	0.03	0.01	0.03	0.04
Fe^{2+}	0.08	0.07	0.08	0.09	0.08	0.07	0.10	0.05	0.07	0.08	0.05	0.10	0.13	0.17	0.16	0.15	0.17	0.16	0.15	0.15	0.16	0.07	0.06	0.08	0.16	0.15
Mn	-	-	-	-	-	-	-	-	-	-	-	-	-	-	-	-	-	-	-	-	-	-	-	-	0.01	-
Mg	0.99	0.89	0.90	0.89	0.91	0.92	0.92	0.94	0.95	0.98	0.94	0.93	1.10	1.64	1.66	1.67	1.64	1.56	1.64	1.60	1.65	1.08	0.94	0.90	1.69	1.68
Ca	0.75	0.86	0.85	0.84	0.82	0.82	0.81	0.82	0.80	0.76	0.82	0.78	0.60	0.07	0.06	0.06	0.07	0.15	0.07	0.13	0.06	0.70	0.87	0.90	0.06	0.08
Na	0.02	0.02	0.02	0.02	0.02	0.02	0.02	0.02	0.02	0.02	0.01	0.02	0.01	-	-	-	-	-	-	-	-	0.02	0.02	0.02	-	-
K	-	-	-	-	-	-	-	-	-	-	-	-	-	-	-	-	-	-	-	-	-	-	-	-	-	-
Ni	-	-	-	-	-	-	-	-	-	-	-	-	-	-	-	-	-	-	-	-	-	-	-	-	-	-
Sum	4.00	4.00	4.00	4.00	4.00	4.00	4.00	4.00	4.00	4.00	4.00	4.00	4.00	4.00	4.00	4.00	4.00	4.00	4.00	4.00	4.00	4.00	4.00	4.00	4.00	4.00
Wollastonite	40.64	46.60	46.32	46.16	44.76	44.64	44.12	44.05	43.39	41.06	44.19	42.97	32.56	3.56	3.20	3.05	3.56	7.92	3.86	6.62	3.24	36.79	45.81	47.76	2.98	4.29
Enstatite	53.69	48.53	48.86	48.76	49.75	50.00	50.36	50.93	51.22	53.21	50.43	51.22	59.90	87.08	87.50	87.44	87.08	83.22	86.44	84.18	86.99	56.86	49.30	47.40	86.76	85.83
Ferrosillite	5.67	4.88	4.82	5.08	5.49	5.36	5.52	5.01	5.39	5.73	5.38	5.81	7.55	9.36	9.29	9.50	9.36	8.86	9.70	9.20	9.77	6.35	4.89	4.85	10.25	9.88
Mg#	92.52	92.71	91.84	90.82	91.92	92.93	90.20	94.95	93.14	92.45	94.95	90.29	89.43	90.61	91.21	91.76	90.61	90.70	91.62	91.43	91.16	93.91	94.00	91.84	91.35	91.80
Cr#	0.10	0.11	0.11	0.11	0.10	0.11	0.10	0.11	0.11	0.11	0.10	0.10	0.10	0.10	0.10	0.10	0.10	0.09	0.10	0.10	0.09	0.15	0.18	0.17	0.17	0.17

Table 4. Microprobe and LA-ICP-MS data for clinopyroxene from Darreh Deh metamorphosed lherzolite. Chondrite normalization factors are from McDonough & Sun (1995).

Note: Eu/Eu*= $Eu_n/(Sm_n+Gd_n)^{0.5}$

	Darreh Deh					Data from Pirnia (2007)									
Sample no.	901*	902*	903*	904*		Cpx -1	Cpx -2	Cpx -3	Cpx -4	Cpx -5	Cpx -6	Cpx -7	Cpx -8	Cpx -9	
(g/100g)															
SiO_2	51.94	51.84	51.62	51.76		51.75	50.98	50.08	50.96	50.38	50.71	50.28	51.15	49.49	
TiO_2	0.13	0.17	0.14	0.16		0.16	0.09	0.20	0.09	0.19	0.21	0.16	0.15	0.18	
Al_2O_3	5.80	5.88	5.76	6.04		5.11	5.53	5.86	5.49	5.49	6.12	5.52	5.70	5.48	
Cr_2O_3	1.10	1.14	1.07	1.10		0.87	1.08	1.15	1.15	1.03	1.12	1.17	1.06	1.08	
FeO	2.99	2.86	2.90	3.41		3.71	3.75	2.72	3.08	2.82	2.95	2.75	3.28	2.77	
MnO	0.10	0.09	0.08	0.08		0.09	0.06	0.09	0.12	0.11	0.14	0.15	0.12	0.09	
MgO	16.63	16.78	16.62	18.57		18.99	18.85	16.24	17.26	16.29	16.73	16.22	17.90	17.60	
CaO	21.90	22.13	22.20	19.56		17.97	18.71	21.74	20.41	20.74	20.60	22.44	19.45	20.37	
Na_2O	0.29	0.26	0.26	0.22		0.35	0.31	0.46	0.36	0.43	0.41	0.42	0.37	0.33	
NiO	0.01	-	-	-		0.11	0.09	0.04	0.04	0.01	0.06	0.04	0.07	0.07	
Sum	100.92	101.18	100.71	100.96		99.11	99.44	98.58	98.99	97.49	99.04	99.14	99.24	97.45	
(μg/g)															
Li	2.604	1.685	1.411	1.509		3.054	2.302	3.918	3.724	3.654	2.644	3.364	3.174	2.500	
Rb	0.079	0.031	0.081	0.206		< 0.027	< 0.034	< 0.033	< 0.019	< 0.065	0.215	< 0.008	< 0.013	< 0.011	
Sr	0.316	< 0.161	0.238	1.037		0.135	0.108	0.318	0.421	1.441	0.466	0.435	0.71	0.361	
Y	6.905	6.869	7.127	6.707		7.462	7.358	7.498	8.308	7.446	7.167	8.259	7.88	7.939	
Zr	0.196	0.180	0.215	0.204		0.358	0.378	0.4	0.453	0.445	0.391	0.435	0.427	0.419	
Nb	0.080	0.086	0.090	0.081		0.059	0.052	0.05	0.064	0.073	0.075	0.057	0.073	0.065	
Ba	0.146	0.111	0.153	0.923		0.029	< 0.026	0.16	0.121	0.537	0.128	0.198	0.374	0.143	
La	< 0.001	< 0.001	< 0.002	< 0.001		< 0.000	< 0.002	< 0.002	< 0.001	< 0.000	< 0.000	< 0.001	< 0.001	< 0.002	
Ce	< 0.002	< 0.003	< 0.002	< 0.002		< 0.003	< 0.001	< 0.005	< 0.001	< 0.003	< 0.003	< 0.004	< 0.003	< 0.004	
Pr	< 0.005	0.005	< 0.003	< 0.004		< 0.008	< 0.004	< 0.011	< 0.010	< 0.007	< 0.007	< 0.009	< 0.011	< 0.006	
Nd	0.096	0.100	0.097	0.092		0.195	0.201	0.172	0.196	0.186	0.206	0.223	0.214	0.227	
Sm	0.207	0.209	0.220	0.214		0.269	0.312	0.287	0.318	0.281	0.301	0.321	0.305	0.281	
Eu	0.109	0.105	0.114	0.107		0.154	0.119	0.124	0.161	0.138	0.135	0.159	0.164	0.147	
Ti	761	1019	833	941		516	1217	516	1145	1259	941	917	1103		
Gd	0.610	0.571	0.636	0.593		0.713	0.710	0.761	0.826	0.745	0.720	0.818	0.845	0.787	
Tb	0.136	0.132	0.141	0.141		0.18	0.141	0.144	0.158	0.162	0.153	0.18	0.181	0.175	
Dy	1.135	1.159	1.224	1.144		1.224	1.318	1.32	1.466	1.325	1.204	1.435	1.406	1.358	
Ho	0.263	0.272	0.291	0.268		0.303	0.285	0.286	0.324	0.285	0.288	0.342	0.321	0.323	
Er	0.789	0.794	0.837	0.787		0.89	0.837	0.861	0.965	0.884	0.818	0.981	0.956	0.861	
Tm	0.120	0.120	0.122	0.109		0.12	0.134	0.137	0.133	0.119	0.127	0.142	0.145	0.14	
Yb	0.795	0.792	0.880	0.762		0.717	0.904	0.754	1.017	0.807	0.811	0.95	0.955	0.906	
Lu	0.116	0.111	0.120	0.104		0.107	0.113	0.109	0.119	0.116	0.115	0.132	0.121	0.11	
Hf	< 0.047	< 0.048	< 0.056	< 0.057		0.055	0.055	0.078	0.092	0.083	0.086	0.095	0.08	0.088	
Ta	< 0.002	< 0.001	< 0.004	< 0.003		< 0.003	< 0.004	< 0.005	< 0.001	< 0.001	< 0.002	< 0.004	< 0.002	< 0.002	
K	50	-	-	-		66	-	224	-	-	8	-	-	-	
Pb	< 0.013	< 0.014	< 0.011	< 0.018		< 0.038	< 0.059	< 0.078	< 0.087	< 0.113	< 0.090	< 0.046	< 0.038	< 0.040	
Th	< 0.002	< 0.003	< 0.001	< 0.001		< 0.004	< 0.002	< 0.009	< 0.003	< 0.000	< 0.000	< 0.002	< 0.001	< 0.001	
Ratios:					Average:										*Average:*
Eu/Eu*	0.94	0.93	0.93	0.92	0.93	1.07	0.77	0.81	0.96	0.92	0.88	0.95	0.98	0.95	0.92
Sm_n/Lu_n	0.3	0.31	0.3	0.34	0.31	0.42	0.46	0.44	0.44	0.4	0.44	0.4	0.42	0.42	0.43

Table 5. Representative microprobe data for chromian spinel in Darreh Deh metamorphosed peridotites and their calculated structural formula based on 32 oxygen atoms.
Note: F = 10xln (Cr#$_{\text{Spinel}}$)+24; *: Data from PIRNIA (2007).

Rock sample	Lhz	Lhz	Lhz	Lhz	Lhz	Lhz	Lhz	Lhz	Lhz	Lhz	Lhz	Lhz	lhz*	lhz*	Hz	Hz*	Hz*	Hz*
Point No.	20	55	56	57	82	83	84	289	290	292	293	301	68	69	330	46	47	48
(g/100g)																		
SiO_2	0.00	0.00	0.00	0.00	0.00	0.00	0.00	0.00	0.00	0.00	0.00	0.00	0.00	0.00	0.00	0.02	0.01	0.00
TiO_2	0.05	0.04	0.05	0.03	0.05	0.06	0.07	0.04	0.04	0.05	0.03	0.04	0.05	0.07	0.22	0.05	0.02	0.04
Al_2O_3	48.75	48.54	48.66	48.66	49.10	49.23	49.45	48.05	49.00	48.74	48.59	48.13	49.13	50.36	26.31	32.95	33.25	32.76
Cr_2O_3	19.62	19.24	19.27	19.34	19.44	19.67	19.20	18.14	17.95	18.90	19.14	18.82	18.81	17.64	37.01	34.83	34.50	34.75
FeO	12.05	13.30	13.48	13.49	12.07	11.94	12.25	12.89	13.04	11.83	11.80	13.05	12.79	12.47	23.06	16.17	15.83	16.11
MnO	0.16	0.13	0.13	0.18	0.13	0.15	0.11	0.14	0.10	0.16	0.16	0.14	0.14	0.12	0.30	0.20	0.21	0.20
MgO	18.65	18.26	18.30	18.32	18.91	19.21	19.14	18.34	18.46	19.30	19.19	18.98	18.27	18.39	11.50	15.21	15.41	14.71
CaO	0.00	0.00	0.02	0.01	0.01	0.01	0.01	0.00	0.01	0.00	0.02	0.01	0.01	0.02	0.00	0.01	0.02	0.00
Na_2O	0.00	0.00	0.01	0.00	0.00	0.00	0.00	0.03	0.01	0.02	0.00	0.00	0.00	0.00	0.04	0.00	0.00	0.00
K_2O	0.00	0.00	0.00	0.00	0.00	0.00	0.00	0.00	0.00	0.00	0.00	0.00	0.00	0.00	0.00	0.00	0.00	0.00
NiO	0.28	0.26	0.30	0.28	0.25	0.29	0.29	0.25	0.24	0.30	0.29	0.26	0.00	0.00	0.12	0.00	0.00	0.00
Sum	99.55	99.77	100.21	100.32	99.96	100.56	100.52	97.88	98.85	99.29	99.23	99.43	99.20	99.05	98.55	99.44	99.24	98.56
(a.p.f.u.)																		
Si	0.00	0.00	0.00	0.00	0.00	0.00	0.00	0.00	0.00	0.00	0.00	0.00	0.00	0.00	0.00	0.00	0.00	0.00
Ti	0.01	0.01	0.01	0.01	0.01	0.01	0.01	0.01	0.01	0.01	0.01	0.01	0.01	0.01	0.04	0.01	0.00	0.01
Al	12.42	12.38	12.37	12.35	12.44	12.39	12.44	12.44	12.54	12.39	12.37	12.27	12.54	12.80	7.66	9.07	9.14	9.11
Cr	3.35	3.29	3.29	3.29	3.30	3.32	3.24	3.15	3.08	3.23	3.27	3.22	3.22	3.01	7.23	6.43	6.36	6.48
Fe^{3+}	0.21	0.31	0.33	0.34	0.25	0.27	0.29	0.39	0.36	0.37	0.35	0.50	0.23	0.17	1.02	0.48	0.49	0.39
Fe^{2+}	1.97	2.09	2.10	2.09	1.92	1.86	1.90	1.97	2.01	1.77	1.79	1.86	2.09	2.08	3.74	2.68	2.60	2.79
Mn	0.03	0.02	0.02	0.03	0.02	0.03	0.02	0.03	0.02	0.03	0.03	0.03	0.03	0.02	0.06	0.04	0.04	0.04
Mg	6.01	5.89	5.88	5.88	6.06	6.12	6.09	6.01	5.98	6.21	6.18	6.12	5.90	5.91	4.24	5.29	5.33	5.18
Ca	0.00	0.00	0.00	0.00	0.00	0.00	0.00	0.00	0.00	0.00	0.01	0.00	0.00	0.00	0.00	0.00	0.01	0.00
Na	0.00	0.00	0.00	0.00	0.00	0.00	0.00	0.00	0.00	0.00	0.00	0.00	0.00	0.00	0.00	0.00	0.00	0.00
K	0.00	0.00	0.00	0.00	0.00	0.00	0.00	0.00	0.00	0.00	0.00	0.00	0.00	0.00	0.00	0.00	0.00	0.00
Ni	0.01	0.01	0.01	0.01	0.00	0.01	0.01	0.00	0.00	0.01	0.01	0.01	0.00	0.00	0.00	0.00	0.00	0.00
Sum	24.01	24.01	24.01	24.01	24.00	24.01	24.01	24.01	24.01	24.01	24.01	24.01	24.00	24.00	24.00	24.00	24.00	24.00
Cr#	0.21	0.21	0.21	0.21	0.21	0.21	0.21	0.20	0.20	0.21	0.21	0.21	0.20	0.19	0.49	0.41	0.41	0.42
Mg#	0.75	0.74	0.74	0.74	0.76	0.77	0.76	0.75	0.75	0.78	0.78	0.77	0.74	0.74	0.53	0.66	0.67	0.65
F	8.52	8.39	8.39	8.42	8.39	8.46	8.23	8.01	7.77	8.22	8.35	8.29	7.91	7.39	16.77	15.08	15.08	15.32

Table 6. Representative microprobe data for amphibole (T: tremolite, TH: tremolitic hornblende; classification of Leake et al. 1997), chlorite (C: clinochlore, TC: talc-chlorite; classification of Hey 1954), and serpentine (L: lizardite, C: chrysotile, based on Raman spectrometry) and the calculated structural formula based on 23, 28 and 7 oxygen atoms, respectively (Darreh Deh metamorphosed lherzolite).

Mineral type	amphibole								chlorite				serpentine					
Sample no.	87	99	304	306	79	98	81	295	291	101	90	91	74	75	297	303	64	65
(g/100g)																		
SiO_2	54.50	57.02	56.31	55.16	53.11	54.05	54.23	54.16	33.66	33.55	37.77	37.52	54.43	50.93	43.83	45.81	34.82	36.09
TiO_2	0.08	0.06	0.04	0.10	0.14	0.16	0.04	0.12	0.02	0.00	0.09	0.07	0.02	0.01	0.02	0.06	0.00	0.00
Al_2O_3	2.54	0.98	2.81	3.33	5.51	3.57	4.48	3.79	13.77	15.35	6.36	5.82	3.49	2.84	5.05	5.98	0.00	0.00
Cr_2O_3	0.57	0.28	0.27	0.49	0.94	1.02	0.22	1.37	0.10	0.04	1.42	1.27	0.69	0.59	0.43	0.89	0.00	0.00
FeO	3.01	2.63	1.82	1.88	2.43	3.13	2.42	2.64	2.47	3.23	4.72	4.69	1.60	2.45	3.55	2.04	7.03	7.42
MnO	0.10	0.12	0.03	0.02	0.04	0.07	0.07	0.05	0.01	0.01	0.03	0.03	0.00	0.03	0.01	0.02	0.09	0.10
MgO	23.95	22.99	22.78	22.00	20.98	21.71	22.36	21.75	32.96	33.40	35.04	34.84	30.80	31.99	31.67	32.37	39.67	37.95
CaO	10.08	12.68	13.53	13.45	13.38	12.55	12.36	13.07	bd	0.01	0.01	0.01	0.06	0.09	0.14	0.03	0.06	0.04
Na_2O	0.62	0.25	0.45	0.49	0.81	0.81	0.71	0.57	bd	bd	0.01	bd	0.12	0.03	0.04	0.08	bd	bd
K_2O	0.02	0.01	0.03	0.02	0.02	0.02	0.03	0.03	0.01	bd	0.01	0.02	0.02	0.04	0.01	0.01	bd	bd
NiO	0.06	0.07	0.07	0.07	0.07	0.06	0.08	0.07	bd	bd	bd	bd	0.13	0.11	0.11	0.16	0.33	0.31
Sum	95.53	97.09	98.16	97.00	97.43	97.14	96.98	97.61	83.00	85.59	85.43	84.26	91.35	89.12	84.86	87.43	81.99	81.92
(a.p.f.u.)																		
Si	7.64	7.82	7.67	7.63	7.36	7.47	7.46	7.45	6.59	6.40	7.30	7.36	2.33	2.26	2.08	2.09	1.81	1.87
Ti	0.01	0.01	0.01	0.01	0.01	0.02	0.01	0.01	0.00	0.00	0.01	0.01	0.00	0.00	0.00	0.00	0.00	0.00
Al^{total}	-	-	-	-	-	-	-	-	-	-	-	-	0.18	0.15	0.28	0.32	0.00	0.00
Al^{IV}	0.36	0.16	0.33	0.37	0.64	0.53	0.54	0.55	1.41	1.60	0.70	0.65	-	-	-	-	-	-
Al^{VI}	0.06	-	0.12	0.17	0.26	0.05	0.19	0.06	1.76	1.85	0.75	0.70	-	-	-	-	-	-
Cr	0.06	0.03	0.03	0.05	0.10	0.11	0.02	0.15	0.02	0.01	0.22	0.20	0.02	0.02	0.02	0.03	-	-
Fe^{total}	-	-	-	-	-	-	-	-	-	-	-	-	0.06	0.09	0.14	0.08	0.31	0.32
Fe^{3+}	0.00	0.30	0.10	-	0.06	0.36	0.28	0.30	-	-	-	-	-	-	-	-	-	-
Fe^{2+}	0.35	-	0.11	0.22	0.22	-	-	-	0.41	0.52	0.76	0.77	-	-	-	-	-	-
Mn	0.01	0.01	-	-	0.01	0.01	0.01	0.01	-	-	-	0.01	-	-	-	-	-	0.01
Mg	5.01	4.70	4.63	4.54	4.33	4.47	4.59	4.46	9.62	9.50	10.10	10.18	1.97	2.12	2.24	2.20	3.07	2.93
Ca	1.51	1.86	1.98	1.99	1.99	1.86	1.82	1.93	-	-	-	-	-	-	0.01	-	-	-
Na	0.17	0.07	0.12	0.13	0.22	0.22	0.19	0.15	-	-	-	-	0.01	-	-	0.01	-	-
K	-	-	0.01	-	-	-	0.01	-	-	-	-	-	-	-	-	-	-	-
Ni	-	0.01	0.01	0.01	0.01	0.01	0.01	0.01	-	-	-	-	-	-	-	0.01	0.01	0.01
Sum	15.19	14.96	15.10	15.13	15.21	15.10	15.12	15.08	19.77	19.85	19.81	19.83	4.57	4.66	4.77	4.74	5.20	5.13
Mg#	93.47	-	97.68	95.38	95.16	-	-	-	95.91	94.81	93.00	92.97	-	-	-	-	-	-
Fe#	-	-	-	-	-	-	-	-	0.04	0.05	0.07	0.07	-	-	-	-	-	-
Cr#	-	-	-	-	-	-	-	-	-	-	-	-	0.12	0.12	0.94	0.09	-	-
Mineral Classification	T	T	T	T	TH	TH	TH	TH	C	C	TC	TC	C	C	C	C	L	L
Product of:	Cpx	Cpx	Opx	Opx	Cpx	Cpx	Opx	Opx	Cr-Spl	Cr-Spl	Cpx	Cpx	Opx	Opx	Opx	Opx	Ol	Ol

Table 7. Bulk rock compositions of metamorphosed Darreh Deh metamorphosed mantle peridotites (major element oxides, V, Cr and Zn obtained by XRF; the other elements obtained by ICP-MS). * = XRF data of mantle peridotite from Torabi (2013), ** = ICP-MS data of mantle peridotite from Ghazi et al. (2011). Abbreviations: meta= metamorphosed, Lhz= lherzolite, Hz= harzburgite, Du = dunite.

Sample no.	L- N223-2	L- N27*	L-N29*	L-N30*	BKB-1 M**	BPV-12M **-	BKB-12 M**	H- N214-2	H-N35*	H-N36*	H-N37*	D- N206-2	D-N38*	D-N39*
Rock type	meta Lhz	Lhz	Lhz	Lhz	Lhz	Lhz	Lhz	meta Hz	Hz	Hz	Hz	meta Du	Du	Du
(g/100g)														
SiO_2	41.18	41.18	39.45	38.63	36.50	39.10	38.67	41.06	38.56	37.81	38.49	39.06	36.90	38.83
TiO_2	bd	bd	bd	bd	0.01	0.03	0.03	bd	bd	bd	bd	bd	bd	bd
Cr_2O_3	0.45	bd	bd	bd	bd	bd	bd	0.41	bd	bd	bd	0.41	bd	bd
Al_2O_3	1.90	1.71	1.48	1.53	1.14	1.99	2.02	0.59	1.07	0.95	0.71	0.39	0.77	0.59
FeO*	7.19	7.02	7.30	6.87	7.63	7.86	8.14	7.41	6.33	6.43	6.06	7.20	6.51	6.07
MnO	0.12	0.13	0.14	0.11	0.10	0.11	0.11	0.12	0.09	0.10	10.00	0.11	0.12	0.11
MgO	38.84	36.90	37.52	38.78	41.70	39.30	37.63	41.77	38.54	37.90	38.63	41.79	38.10	37.92
CaO	2.10	2.24	2.06	1.75	1.15	2.03	3.17	0.64	1.33	1.00	0.91	0.35	0.62	0.51
Na_2O	0.16	0.04	0.03	0.03	0.03	bd	0.01	0.20	0.03	0.02	0.03	0.14	0.01	0.05
K_2O	bd	0.03	0.01	0.01	0.13	0.13	0.88	bd	0.01	bd	0.02	bd	bd	0.01
NiO	0.24	bd	bd	bd	bd	bd	bd	0.27	bd	bd	bd	0.28	bd	bd
P_2O_5	bd	bd	bd	bd	0.01	0.03	0.02	bd	bd	bd	bd	0.01	bd	bd
LOI	8.01	11.24	10.81	10.26	10.79	8.95	9.50	7.68	12.43	12.70	13.09	10.31	12.50	13.49
Sum	100.19	100.49	98.80	97.97	99.19	99.53	100.18	100.15	98.39	96.91	107.94	100.05	95.53	97.58
Mg#	84.38	84.02	83.72	84.96	84.53	83.33	82.22	84.94	85.88	85.49	86.45	85.31	85.40	86.19
(μg/g)														
Be	0.01	-	-	-	-	-	-	0.01	-	-	-	0.01	-	-
Sc	14.02	12	11	10	9	12	14.22	11.3	11	9	8	9.7	7	8
Ti	0.03	-	-	-	-	-	-	0.02	-	-	-	0.01	-	-
V	71.4	53	49	54	4	65	60.84	38.06	45	40	38	34.6	35	40
Cr	3060	-	-	-	1732	2294	2313	2770	-	-	-	2791	-	-
Co	95	110	100	98	11	107	100.93	104	106	115	104	105	115	112
Ni	1896	-	-	-	1851	1809	1551	2114	-	-	-	2170	-	-
Cu	11	-	-	-	3.76	19.1	15.55	1	-	-	-	2.7	-	-
Zn	47.4	-	-	-	57	57	53.9	41.2	-	-	-	34.7	-	-
Ga	2.61	-	-	-	-	-	-	1.29	-	-	-	1.17	-	-
As	0.71	-	-	-	-	-	-	0.26	-	-	-	0.42	-	-
Rb	<0.5	-	-	-	0.22	0.21	0.22	<0.5	-	-	-	<0.5	-	-
Sr	22.6	-	-	-	17	13	16.4	97	-	-	-	11.6	-	-
Y	1.05	-	-	-	0.92	0.93	1.35	0.27	-	-	-	0.17	-	-
Zr	<5	-	-	-	1.74	0.56	1.21	<5	-	-	-	<5	-	-
Nb	<0.1	-	-	-	0.05	0.03	0.03	<0.1	-	-	-	<0.1	-	-
Mo	0.05	-	-	-	-	-	-	<0.05	-	-	-	0.86	-	-
Cd	0.06	-	-	-	-	-	-	0.06	-	-	-	0.05	-	-
Sn	0.3	-	-	-	-	-	-	0.2	-	-	-	0.28	-	-
Sb	0.24	-	-	-	-	-	-	0	-	-	-	0.18	-	-
Cs	0.02	-	-	-	0.02	0.01	0.02	0.01	-	-	-	0.02	-	-
Ba	14.9	-	-	-	-	-	-	8.3	-	-	-	10.1	-	-
La	0.009	<0.16	<0.15	<0.18	0.051	-	-	0.008	<0.10	<0.12	<0.09	0.025	<0.08	<0.12
Ce	<0.02	-	-	-	0.125	-	0.080	<0.02	-	-	-	<0.02	-	-
Pr	0.009	-	-	-	0.012	0.001	0.009	0.009	-	-	-	0.014	-	-
Nd	0.054	-	-	-	0.082	0.023	0.067	0.050	-	-	-	0.071	-	-
Sm	0.021	<0.12	<0.12	<0.10	0.031	0.015	0.034	0.017	<0.10	<0.12	<0.09	0.002	<0.08	<0.12
Eu	0.015	-	-	-	0.008	0.014	0.019	0.005	-	-	-	0.008	-	-
Gd	0.079	-	-	-	0.032	0.052	0.065	0.027	-	-	-	0.018	-	-
Tb	0.020	-	-	-	0.007	0.016	0.013	0.005	-	-	-	0.004	-	-
Dy	0.151	<0.20	<0.18	<0.20	0.080	0.126	0.131	0.042	<0.25	<0.20	<0.24	0.027	<0.20	<0.22
Ho	0.039	-	-	-	0.021	0.035	0.032	0.012	-	-	-	0.005	-	-
Er	0.126	-	-	-	0.068	0.124	0.101	0.034	-	-	-	0.022	-	-
Tm	0.021	-	-	-	0.008	0.027	0.019	0.005	-	-	-	0.002	-	-
Yb	0.144	<0.10	<0.10	<0.09	0.084	0.170	0.124	0.043	<0.10	<0.11	<0.10	0.023	<0.10	<0.12
Lu	0.022	-	-	-	0.015	0.028	0.020	0.008	-	-	-	0.005	-	-
Hf	-	-	-	-	0.03	0.02	0.03	-	-	-	-	-	-	-
Ta	<0.005	-	-	-	-	-	-	<0.005	-	-	-	<0.005	-	-
W	0.2	-	-	-	-	-	-	0.01	-	-	-	0.05	-	-
Pb	0.12	-	-	-	1.52	1.63	1.61	<0.1	-	-	-	2.21	-	-
Th	<0.005	-	-	-	0.05	0.02	0.03	<0.005	-	-	-	<0.005	-	-
U	0.01	-	-	-	-	-	-	<0.005	-	-	-	<0.005	-	-
Eu/Eu*	1.52	-	-	-	-	-	-	1.24	-	-	-	1.76	-	-
La_n/Yb_n	0.05	-	-	-	0.41	-	-	0.17	-	-	-	0.68	-	-
La_n/Sm_n	0.31	-	-	-	1.03	-	-	0.31	-	-	-	1.25	-	-
Gd_n/Yb_n	0.46	-	-	-	0.31	0.25	0.42	0.61	-	-	-	1.21	-	-
ΣREE	0.710	-	-	-	0.624	0.631	0.714	0.265	-	-	-	0.226	-	-

Table 8. Calculated K_d and melt compositions for Darreh Deh mantle lherzolite based on clinopyroxene composition (data from Table 3) using the method of Wood & Blundy (1997).

	La	Ce	Pr	Nd	Sm	Eu	Gd	Tb	Dy	Y	Ho	Er	Tm	Yb	Lu
Average K_d	0.283	0.453	0.676	0.945	1.458	1.656	1.817	1.926	1.974	1.972	1.962	1.905	1.819	1.718	1.614
Melt 901	0.004	0.004	0.007	0.102	0.142	0.066	0.336	0.071	0.575	3.501	0.134	0.414	0.066	0.463	0.072
Melt 902	0.004	0.007	0.007	0.106	0.143	0.063	0.314	0.069	0.587	3.483	0.139	0.417	0.066	0.461	0.069
Melt 903	0.007	0.004	0.004	0.103	0.151	0.069	0.350	0.073	0.620	3.614	0.148	0.439	0.067	0.512	0.074
Melt 904	0.004	0.004	0.006	0.097	0.147	0.065	0.326	0.073	0.579	3.401	0.137	0.413	0.060	0.444	0.064